



UNIVERSITÀ DEGLI STUDI DI MILANO

Facoltà di Scienze e Tecnologie
Corso di Laurea Triennale in Fisica

**IMPACT OF THEORETICAL
UNCERTAINTIES ON PDFs ON HIGGS
CROSS SECTION**

Relatore:
Stefano Forte

Candidato:
Andrea Isgrò
Matricola n. 775208

Anno Accademico 2012-2013

Summary

The purpose of this thesis is to analyse the PDF (Parton Distribution Functions) dependence of the Higgs cross section in gluon fusion, and in particular to investigate how theoretical uncertainties on parton distributions affect the perturbative series for this process.

First, the Higgs boson is briefly introduced in Chapter 1, with specific reference to its production at LHC. The computation of its cross section requires perturbative matrix elements and PDFs.

Parton Distribution Functions, the momentum distribution functions of the partons within the hadrons, are related to the Higgs cross section via the factorization theorems. In Chapter 2 it is shown how the PDFs can be extracted from experimental data and what are the main ways to compute their uncertainties.

There is a source of uncertainty which arises from the neglect of higher order terms in QCD perturbative computations. It shall be called Theoretical Uncertainty, in opposition to Statistical Uncertainty (or simply PDF uncertainty), which follows from error propagations of the experimental data used for the PDF determination.

Chapter 3 deals with the conventional method to estimate theoretical uncertainties in perturbative series and presents the Cacciari-Houdeau model, which assigns a meaningful degree of belief to those estimates [13].

Once made the assumption that PDFs which belong to different-order sets are, point by point, a perturbative series in α_S , theoretical C-H uncertainties on PDFs are computed and compared with statistical uncertainties. The same exercise is repeated for Parton Luminosities, defined in Section 3.5.

Finally, in Chapter 4, two codes (ggHiggs [16] and iHixs [17]) are used to obtain the Higgs cross section, which depends on the PDF set considered. This dependence is exploited to estimate the impact of theoretical uncertainties of PDFs themselves on Higgs cross section, which can be compared to theoretical uncertainties on gluon-gluon luminosity.

The scaled parameter Cacciari-Houdeau model is used to compute theoretical uncertainties on the Higgs production perturbative series (using the best PDF set available), and compared to the standard methodology, based on scale variation.

Contents

1	The Higgs Boson	4
1.1	Properties	4
1.2	Decay channels and branching ratios	4
1.2.1	Fermion-antifermion	6
1.2.2	Pair of massive bosons	6
1.2.3	Pair of massless bosons	6
1.3	Higgs production at LHC	6
1.3.1	Gluon-gluon fusion	6
1.3.2	WW, ZZ fusion	7
1.3.3	Associated production with W, Z bosons	7
1.3.4	Associated production with $t\bar{t}$	7
2	Parton Distribution Functions	9
2.1	PDF definition	9
2.2	PDF Sets	10
2.3	Determination of PDFs	10
2.3.1	Goodness of fit	11
2.3.2	Parton parametrization	11
2.4	Computation of Statistical Uncertainties	12
2.4.1	The Hessian approach	12
2.4.2	The Monte Carlo approach	13
3	Theoretical Uncertainties	14
3.1	Perturbative Series in QCD	14
3.2	Scale variation	15
3.3	The Cacciari-Houdeau Method	16
3.3.1	Model hypotheses	17
3.3.2	Model Outcomes	18
3.4	Example: PDFs	19
3.4.1	Leading Order	20
3.4.2	Next to Leading Order	21
3.4.3	Next to Next to Leading Order	22
3.4.4	Choice of the expansion parameter α_S	25
3.4.5	Impact of Statistical Uncertainty	25
3.5	Example: Parton Luminosities	25
3.5.1	Definition	25
3.5.2	Perturbative series	26

3.5.3	Results for M_X	26
3.5.4	Results for $M_X = m_H$	26
4	Theoretical Uncertainties on Higgs Cross Section	29
4.1	ggHiggs and iHixs	29
4.2	Fixed Cross Section	30
4.3	Fixed PDF	32
4.4	The parameter λ	34
4.5	Series starting at $l = 1$	34
4.6	Comparison with scale variation	39
4.7	PDF impact	39
4.8	Concluding remarks	41

Chapter 1

The Higgs Boson

Geneva, 4th July 2012. At a seminar held at CERN, the ATLAS and CMS experiments presented their latest preliminary results in the search for the long sought Higgs particle. Both experiments observed a new particle in the mass region around 125-126 GeV.

On 8th October 2013 François Englert and Peter W. Higgs won the Nobel prize in physics *“for the theoretical discovery of a mechanism that contributes to our understanding of the origin of mass of subatomic particles.”*

This Chapter reviews the main properties of the Standard Model (SM) Higgs Boson and illustrates its most common decay and production channels at LHC.

1.1 Properties

The SM of the electroweak and strong interactions crucially relies on the Higgs mechanism in order to spontaneously break the electroweak symmetry and generate in a gauge invariant way the masses of the elementary particles. In the minimal realization of electroweak symmetry breaking, one complex Higgs doublet field is introduced which implies the existence of a single neutral scalar particle, the Higgs boson H .

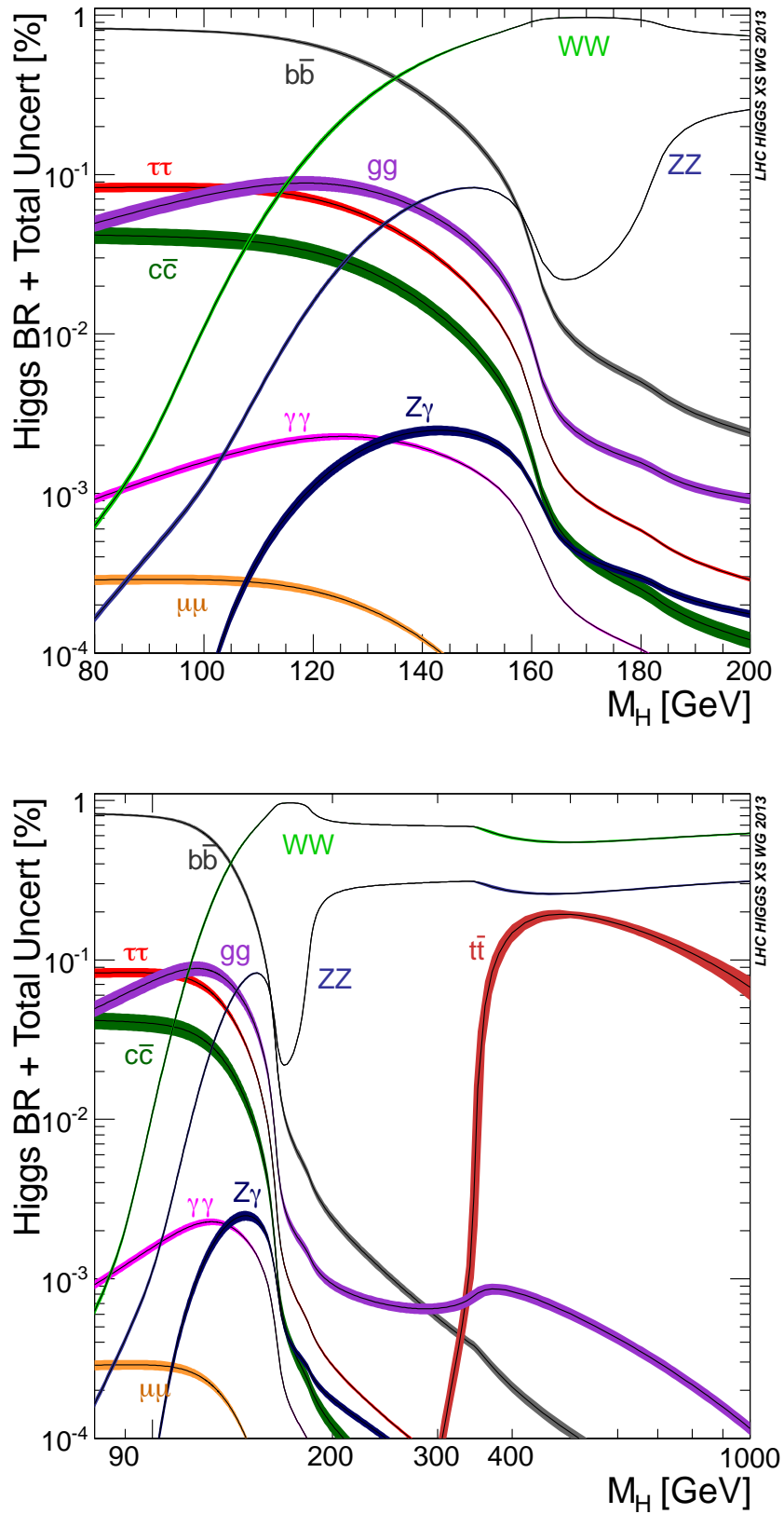
The Higgs is a scalar field (it does not transform under Lorentz transformations), i.e. it has spin 0. It is also its own antiparticle, CP-even, and has zero electric and colour charge. The Minimal Standard Model does not predict the mass of the Higgs boson.

Its spin and parity have been successfully studied on the 125 GeV new particle. These tests are performed by observing the Higgs boson decay products and comparing them with theoretical expectations. This is the reason why more and more accurate calculations of Higgs production and decay cross sections are required.

1.2 Decay channels and branching ratios

According to the Standard Model, the Higgs Boson has several possible decay processes [1], each of which has its own probability. This probability is expressed as a branching ratio: the fraction of particle which decay by an individual decay mode with respect to the total number of decays. The SM predicts these branching ratios as a function of the Higgs mass (see Figure 1.1).

The most relevant decay channel are illustrated below, together with some branching ratio values for a Higgs mass of 125 GeV (data refer to [2]).

Figure 1.1: Decay branching ratios for Higgs at different ranges of M_H .

1.2.1 Fermion-antifermion

One of the most likely decay for the Higgs boson is into a $f\bar{f}$ pair. Since the strength of the interaction between the Higgs and a fermion is proportional to the mass of the fermion, one could expect the most common decay to be into a $t\bar{t}$ pair.

However, as shown in the second plot of Figure 1.1, this decay is only possible (and become dominant) for a Higgs mass of at least twice the mass of the top quark, i.e. ≈ 346 GeV. For the observed Higgs mass, the most likely event is a decay into a $b\bar{b}$ pair (56%). The second most common fermion decay is into a $\tau\bar{\tau}$ pair (6%).

1.2.2 Pair of massive bosons

The Higgs Boson can also decay into a pair of massive gauge bosons, such as WW or ZZ . The former is more common, as it happens 23% of the time, but it is also the most difficult to distinguish from the background. In fact, W often decays again into a quark-antiquark pair or into a charged lepton and a neutrino, which makes it almost impossible to fully reconstruct the event.

The decay into a pair of Z is instead easier to detect, as each of the bosons can subsequently decay into a pair of charged leptons, but its occurrence is about 2.9%.

1.2.3 Pair of massless bosons

Finally, decay into gluons or photons is also possible, but it has to be mediated by a loop of virtual heavy quarks or massive gauge bosons. The most common of this kind of processes (8.5%) is the opposite of the gluon fusion which will be described in Section 1.3.1, namely the decay into a pair of gluons through a loop of virtual heavy quarks, such as t or b .

Another option is to decay into a pair of photons mediated by a loop of W bosons or heavy quarks. This process is rare (the pink line in Figure 1.1) but highly relevant, as the energy and momentum of the photons can be measured very precisely, giving an accurate reconstruction of the mass of the decaying particle.

1.3 Higgs production at LHC

The Standard Model predicts that the Higgs boson can be produced in a number of ways, with probabilities depending on its mass value. In particular, we consider Higgs production for the LHC proton-proton collider with $\sqrt{s} = 8$ TeV and 14 TeV. A high center of mass energy is preferred because light bosons are copiously produced but suffer from severe backgrounds, while heavier Higgs bosons have smaller production cross sections but with more manageable backgrounds.

There are only a limited number of production mechanisms which give cross sections large enough to be relevant at LHC, as illustrated in Figure 1.6 (data from [2]). Each of the most relevant processes is described below, together with its Leading Order Feynman diagram.

1.3.1 Gluon-gluon fusion

The most relevant channel in Higgs production is gluon fusion $pp \rightarrow H$, in which two gluons, one from each proton, combine to form a loop of virtual quarks. In other words, the gluons do not directly interact with each other, but rather with quarks and anti-quarks. Once again, the

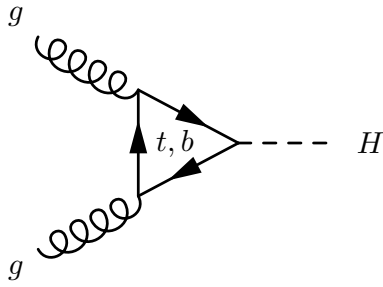
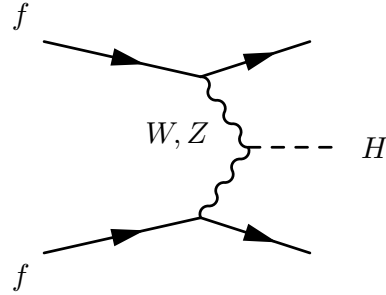
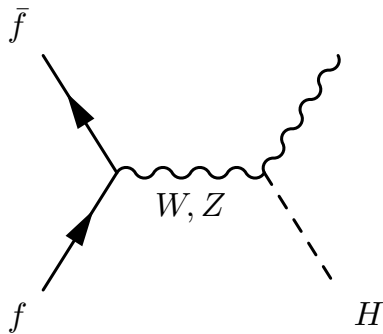
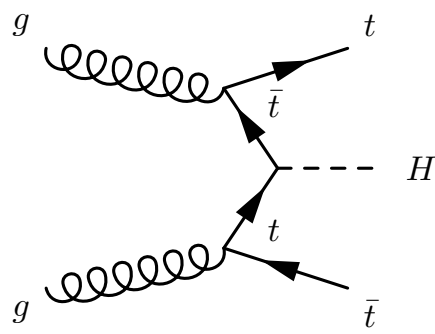


Figure 1.2: Gluon-gluon fusion.

Figure 1.3: WW, ZZ fusion.Figure 1.4: Associated production with W, Z .Figure 1.5: Associated production with $t\bar{t}$.

Higgs boson is more likely to interact with heavy particles, so only top and bottom quarks give a significant contribution. Gluon fusion is the dominant contribution at the LHC, being about ten times more common than any of the other processes.

1.3.2 WW, ZZ fusion

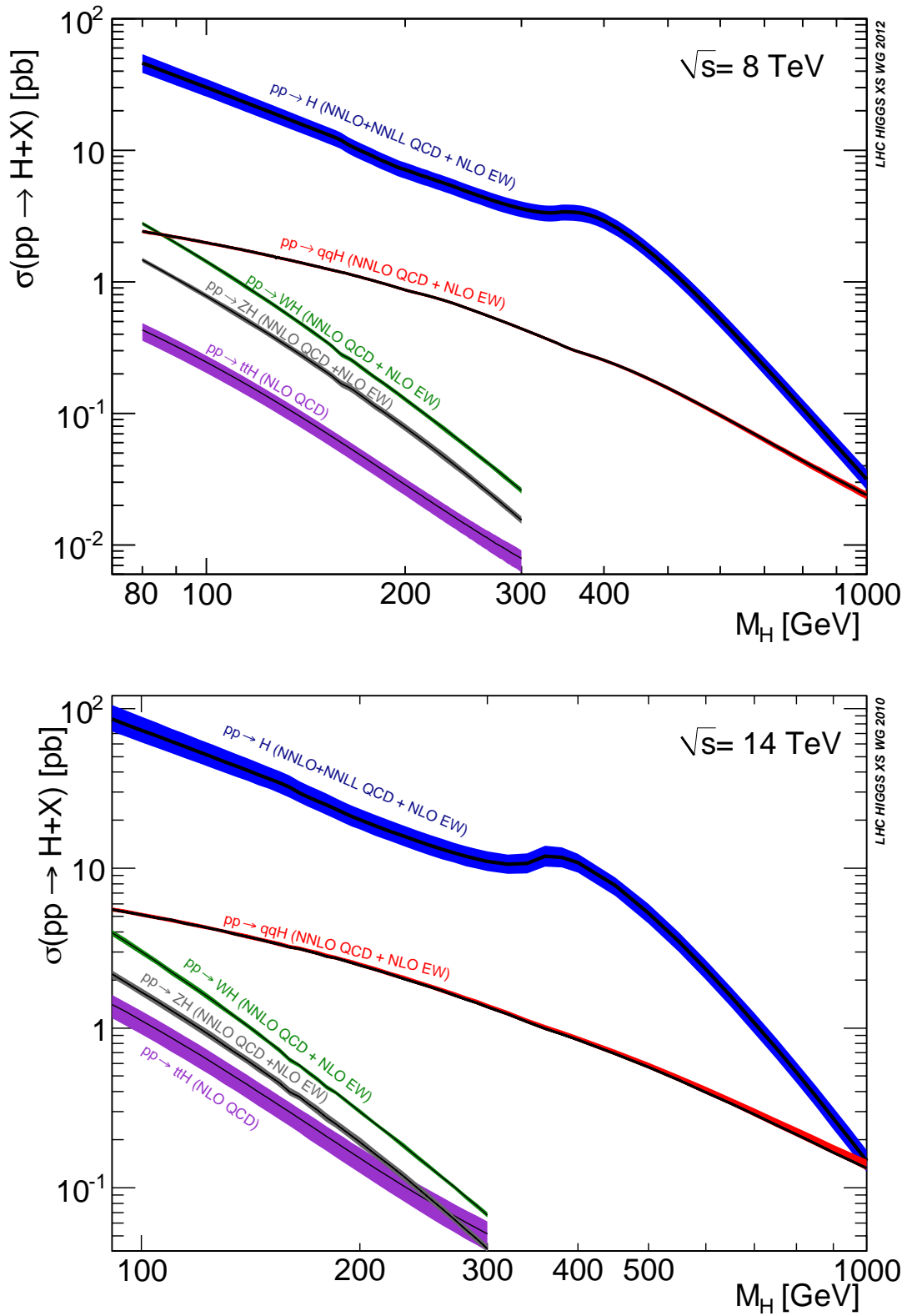
The second most likely event for Higgs production is WW or ZZ fusion $pp \rightarrow qqH$, where two quarks (or antiquarks) create two disturbances in the W (or Z) field. The two virtual bosons then form a Higgs boson. The colliding quarks do not necessarily have to be of the same flavour.

1.3.3 Associated production with W, Z bosons

Other two channel for Higgs production, quite similar to each other, are associated production with W and Z , respectively $pp \rightarrow WH$ and $pp \rightarrow ZH$. In this process, an elementary fermion within a proton collides with its antifermion coming from the other proton, to produce a W or Z virtual boson. Then the virtual boson decays into a Higgs boson and a W or Z particle. The reason why these two processes are considered separately in the plot in Figure 1.6 is that W and Z particles can be distinguished experimentally. The process is also called Higgs Strahlung.

1.3.4 Associated production with $t\bar{t}$

Finally, the least likely event that is usually considered is associated production with $t\bar{t}$, $pp \rightarrow t\bar{t}H$, which is by two order of magnitude less probable than gluon fusion. This process involves two colliding gluons, which each decay into a heavy quark-antiquark pair (e.g. $t\bar{t}$). A top and anti-top from each pair can then combine to form a Higgs particle.

Figure 1.6: Higgs production at $\sqrt{s} = 8$ TeV and $\sqrt{s} = 14$ TeV.

Chapter 2

Parton Distribution Functions

The computation of a cross section at a hadron collider requires the knowledge of the quark and gluon substructure of the colliding hadrons. This is encoded in Parton Distribution Functions (PDFs). It seems appropriate to introduce them, underlining what they represent, how they can be deduced from the data and what are the tools which allow us to assign them uncertainty bands.

2.1 PDF definition

Deep Inelastic Scattering experiments (DIS), in which leptons are scattered off nucleons, let us investigate the inner structure of nucleons, revealing that hadrons are composed of a number of point-like constituents, named partons. If the momentum transferred in the collision is high, the momentum of the parton interacting with the lepton is almost collinear with the nucleon momentum, so that the target can be seen as a stream of partons, each carrying a fraction x of the longitudinal momentum.

The probability density for a parton of flavour i to carry a fraction x of the nucleon momentum at a squared energy scale Q^2 is expressed by Parton Distribution Functions $f_i(x, Q^2)$. At high Q^2 , there is an increasing number of quark-antiquark pairs which carry a low momentum fraction x : the sea quarks. A relevant discovery of the DIS experiments is that the quarks and antiquarks only carry about half of the nucleon momentum, the remainder being carried by the gluons.

Since parton distributions cannot be computed from first principles, they need to be determined by comparing experimental data with predictions which are made using the PDFs themselves. In fact, the factorization theorems allow us to express the cross section of a hard process as a calculable parton interaction convoluted with the parton densities. QCD gives us the Q^2 dependence of the PDFs through the DGLAP equations (Gribov and Lipatov 1972, Altarelli and Parisi 1977 and Dokshitzer 1977), in the domain where perturbative calculations can be applied, that is in the limit where the running coupling constant of $\alpha_S(Q^2)$ is much smaller than one ($\alpha_S(Q^2) \ll 1$). The kernels which provide the rate of evolution in these equations (splitting functions) can be computed as a perturbative expansion in the strong coupling $\alpha_S(Q^2)$, usually called Leading Order (LO), Next to Leading Order (NLO), etc..

2.2 PDF Sets

The determination of PDFs is currently performed by several groups, as discussed in more detail in [3][4]. In this work only the first three of them will be considered, which are based on a wider set of data.

- MSTW [5]
- CT10 [6]
- NNPDF [7]
- HERAPDF
- ABM
- GJR

The MSTW (Martin-Stirling-Thorne-Watt) PDFs are determined from a global analysis of hard scattering data, based on the HERA DIS data as the main input for PDFs at low x , fixed target DIS data in the high- x region, fixed target Drell-Yan (DY) data which help to constrain high- x sea quarks, TEVATRON jet data contributing to high- x gluon PDF and W , Z data which provide an access to the different quark contributions.

The CT10 PDFs are obtained by a global analysis of hard scattering data in the framework of general mass perturbative QCD. This analysis is based on the same data mentioned above (plus the combined HERA I data and more TEVATRON data).

The Neural Net PDF (NNPDF) group parametrize PDFs by training a neural network on Monte Carlo replicas of the experimental data. With such a method NNPDFs are free of assumptions made by other groups. It also includes all above mentioned experimental data and LHC data in the fit. The functional form used for the PDF parametrization, based on neural networks, has a very large number of parameters. Therefore, the best-fit is not determined as an absolute minimum of a figure of merit (such as the χ^2), which would involve also fitting statistical noise, but rather by stopping the minimization before the noise starts being fitted, through a suitable criterion.

PDF sets in LO, NLO and NNLO are available for all of the three sets mentioned above.

2.3 Determination of PDFs

We only provide a brief summary, for a detailed explanation of the current state of the art in the determination of parton distributions, see [8].

Factorization for hadroproduction lets us express the cross section of a process which depends on a single scale M_X^2 as

$$\sigma_X(s, M_X^2) = \sum_{a,b} \int_{\tau}^1 dx_1 dx_2 f_{a/h_1}(x_1, M_X^2) f_{b/h_2}(x_2, M_X^2) \hat{\sigma}_{ab \rightarrow X}(\hat{s}, M_X^2), \quad (2.3.1)$$

where s is the center-of-mass energy of the hadronic collision, $f_{a/h_i}(x_i, M_X^2)$ is the PDF of the quark with flavour a in the i th incoming adron, $\hat{\sigma}_{ab \rightarrow X}$ is the partonic cross section for the production of the final state X , and $\tau \equiv M_X^2/s$ is the scaling variable of the hadronic process.

Partonic cross sections are computed in perturbation theory, using the quark and gluon degrees of freedom of the QCD Lagrangian. They do not depend either on the incoming hadron or on PDFs, therefore they are universal, i.e., independent of the specific process.

As a result, it is possible to compare experimental data with theoretical predictions at some given perturbative order. The outcome of this comparison, together with a good choice of measurable processes in order to maximize the information, enables the determination of PDFs. Finally, thanks to universality, it is possible to determine PDFs using the experimental information on a particular set of processes, and then use them to obtain predictions for different processes.

Equation (2.3.1) can be rewritten as follows:

$$\sigma_X(s, M_X^2) = \sum_{a,b} \sigma_{ab}^0 \int_{\tau}^1 \frac{dx_1}{x_1} \int_{\tau/x_1}^1 \frac{dx_2}{x_2} f_{a/h_1}(x_1, M_X^2) f_{b/h_2}(x_2, M_X^2) C_{ab} \left(\frac{\tau}{x_1 x_2}, \alpha_S(M_X^2) \right), \quad (2.3.2)$$

where the hard coefficient function $C_{ab}(z, \alpha_S(M_X^2))$ is a function of the scale M_X^2 and the dimensionless ratio

$$z = \frac{M_X^2}{\hat{s}} = \frac{\tau}{x_1 x_2}, \quad \tau \equiv \frac{M_X^2}{s}. \quad (2.3.3)$$

Equation (2.3.1) expresses the inclusive cross section in terms of PDFs at the same scale, M_X^2 , at which the cross section is evaluated. However, PDFs at different scales are related by the DGLAP integro-differential equations.

Consequently, the accuracy of the PDFs is limited by the perturbative order both of the coefficient function in equation (2.3.2) and of the splitting functions which enter the evolution equations. Leading order means that both are computed to the lowest nonvanishing order, so for instance, in Higgs production via gluon fusion, splitting functions to order α_S and coefficient functions to order α_S^2 .

2.3.1 Goodness of fit

Parton distributions are determined by comparing theoretical predictions like equation (2.3.1) with experimental data. A confidence interval in the space of PDFs is then determined by minimizing a suitable measure of goodness-of-fit. Since the PDFs space is an infinite-dimensional space of functions, it is necessary to introduce a finite PDF parametrization, for which several choices are possible.

A goodness-of-fit measure can be defined as

$$\chi^2 = \sum_{i,j}^{N_{\text{dat}}} (d_i - \bar{d}_i) V_{ij}^{-1} (d_j - \bar{d}_j), \quad (2.3.4)$$

\bar{d}_i are data, d_i theoretical predictions, N_{dat} is the number of data points and V_{ij} is the experimental covariance matrix.

2.3.2 Parton parametrization

Apart from the functional form and the number of parameters employed, all existing parametrizations differ in the choice of individual linear combinations of PDFs which are parametrized. Once

a suitable set of basis PDFs has been chosen, a standard choice for the functional form, adopted by most PDF fitting groups, is to assume that at some reference scale Q_0^2

$$f_i(x, Q_0^2) = N x^{\alpha_i} (1-x)^{\beta_i} g_i(x), \quad (2.3.5)$$

where $g_i(x)$ tends to a constant for $x \rightarrow 0$ and $x \rightarrow 1$ and usually is a polynomial or the exponential of a polynomial in x or \sqrt{x} . Typical contemporary PDF sets based on this choice of functional form are parametrized by about 20–30 parameters.

A completely different choice is to parametrize PDFs with a general functional form which does not incorporate any theoretical prejudice, like neural networks. NNPDF uses multilayer feed-forward neural networks for PDF parametrization, one for each PDF and all with a fixed number of parameters (200–300). The form of the parametrization is

$$f_i(x, Q_0^2) = c_i(x) NN_i(x), \quad (2.3.6)$$

where $NN_i(x)$ is a neural network, and $c_i(x)$ is a preprocessing function. The fit parameters are the ones which determine the shape of the NN. The preprocessing function is not fitted, but rather chosen randomly in a space of functions of the general form (2.3.5) within some acceptable range of the parameters α_i and β_i , and with $g_i = 1$.

2.4 Computation of Statistical Uncertainties

Due to the different choices of parametrizations and determination procedures performed by the various groups, there are many ways to compute Statistical Uncertainties, of which the most relevant two will be analysed below. The first, the Hessian approach, is based on the standard least-squares method, while the second is the Monte Carlo approach, whereby the probability distribution of PDFs is given by assigning a Monte Carlo sample of N_{rep} PDF replicas.

2.4.1 The Hessian approach

This approach is mostly applied when the parametrization has a small number of parameters. It makes the assumption that the probability distribution in the space of parton distributions is a multi-Gaussian in the space of parameters.

Starting with a parametrized function of the form of equation (2.3.5), the best fit is the point in parameter space at which χ^2 is minimum, while PDF uncertainties are found by diagonalizing the Hessian matrix of second derivatives of the χ^2 at the minimum and then determining the range of each orthonormal eigenvector which corresponds to a prescribed increase of the χ^2 function with respect to the minimum. For Gaussian uncertainties, the 68% (or 1σ) confidence level corresponds to the volume enclosed by the $\chi^2 = \chi_{\text{min}}^2 + 1$ surface.

This is called the Hessian method, because the confidence level is entirely determined by the covariance matrix in parameter space, which is the inverse of the (Hessian) matrix of second derivatives of the χ^2 with respect to the parameters, evaluated at the minimum.

In general, the variation of the χ^2 which corresponds to a 68% confidence (one sigma) should be $\Delta\chi^2 = 1$. However, a larger variation $\Delta\chi^2 = T^2$, with $T > 1$ a tolerance parameter, is sometimes used for more realistic error estimates for fits containing a wide variety of input data.

PDF uncertainties on any observable that depends on the PDFs (and on the PDFs themselves), are then simply found by adding in quadrature the variation by a fixed amount along

the direction of each eigenvector. So in a Hessian approach one delivers a central set of PDFs S_0 , and N_{par} 1σ error sets S_i , corresponding to the variation of each eigenvector in turn.

Therefore the best value of any quantity $F(S)$ which depends on the PDF set, and its 1σ uncertainty, are respectively¹

$$F_0 = F(S_0), \quad (2.4.1)$$

$$\sigma_F = \sqrt{\sum_{i=1}^{N_{\text{par}}} [F(S_i) - F(S_0)]^2}. \quad (2.4.2)$$

The most significant drawback of this whole procedure is that Hessian diagonalization may run out of hand as the number of parameters grows.

2.4.2 The Monte Carlo approach

Within the Monte Carlo approach, the probability distribution of PDFs is given by determining a Monte Carlo sample of N_{rep} PDF replicas S^k . Any feature of the probability distribution can be determined from the sample. Thus, the best value of any function of the PDF set $F(S)$ is now computed as the mean over the replica sample and the 1σ interval as a standard deviation:

$$F_0 = \frac{1}{N_{\text{rep}}} \sum_{k=1}^{N_{\text{rep}}} F(S^k), \quad (2.4.3)$$

$$\sigma_F = \sqrt{\sum_{i=1}^{N_{\text{par}}} \frac{1}{N_{\text{rep}} - 1} [F(S_i) - F(S_0)]^2}. \quad (2.4.4)$$

The main advantages of the Monte Carlo method are the possibility to handle a large number of parameters in the parametrization and the lack of a priori assumptions on the form of the probability distribution in parameter space, which is not required to be a Gaussian as in the Hessian approach.

Among the multiple possible ways of building a sample, one may choose to construct a Monte Carlo representation of the starting data sample. In other words the sample is constructed in such a way that, in the limit $N_{\text{rep}} \rightarrow \infty$, the central value of the i -th data point $\langle d_i \rangle$ is equal to the mean over the N_{rep} values that the i -th point takes in each replica d_i^k , the uncertainty of the same point is equal to the variance over the replicas, and the correlations between any two original data points is equal to their covariance over the replicas, namely

$$\langle d_i \rangle \equiv \frac{1}{N_{\text{rep}}} \sum_{k=1}^{N_{\text{rep}}} d_i^k, \quad (2.4.5)$$

$$\text{cov}_{ij} \equiv \frac{1}{N_{\text{rep}} - 1} \sum_{i=1}^{N_{\text{rep}}} \sum_{j=1}^{N_{\text{rep}}} (d_i^k - \langle d_i \rangle) (d_j^k - \langle d_j \rangle). \quad (2.4.6)$$

From each data replica, a parton distribution is constructed by minimizing a χ^2 function. PDF central values, uncertainties and correlations are then computed by taking means, variances and covariances over this replica sample.

¹Actually, the formula which is often used is somewhat more complex in order to account for asymmetric uncertainties.

Chapter 3

Theoretical Uncertainties

Whenever performing an experiment, such as at LHC, we compare measurements to theoretical calculations and try to find out if they match or not. If they do, we also need to determine with what degree of confidence this statement can be made. If the theory was exact, an interval would be provided around the true theoretical value inside which there is a certain probability (e.g. 68%, 95.4%, 99.7%) for data to be observed. One could then check whether or not the experimental value would lie within that interval.

However, in practice the theory is perturbative in most cases (as Quantum Chromodynamics), which means that theoretical predictions are perturbative series of which only the first terms are known. In this case, a full control of the uncertainty of these predictions becomes of paramount importance, as both the experiment and the theory need to be provided with a meaningful degree of uncertainty in order to determine their agreement. In QCD the issue of theoretical accuracy is pressing, due to the large size of the coupling α_S and therefore its slow perturbative convergence.

Theoretical predictions in QCD contain multiple inputs that must be ultimately extracted from experimental data, like PDFs and the value of α_S , each of which brings an unavoidable source of uncertainty (the Statistical Uncertainty). This kind of uncertainty has been studied in detail during the past several years. A separate issue is the meaning of the Theoretical Uncertainty, given by unknown higher orders in perturbation theory.

3.1 Perturbative Series in QCD

For definiteness, consider the perturbative calculation for the cross section of a process taking place at a hard scale Q ¹:

$$\sigma(Q) = \sum_{n=0}^{\infty} c_n(Q, \mu) \alpha_S^n(\mu), \quad (3.1.1)$$

where μ is an unphysical momentum scale, and the coupling $\alpha_S(\mu)$ evolves according to the DGLAP equations. When no dependence is given explicitly, the coefficients and the coupling will be considered at a scale $\mu = Q$:

$$\sigma(Q) = \sum_{n=0}^{\infty} c_n(Q, Q) \alpha_S^n(Q) = \sum_{n=0}^{\infty} c_n \alpha_S^n. \quad (3.1.2)$$

¹QCD series are not convergent but simply asymptotic. However, since the asymptotic behaviour is supposed to kick in at high perturbative order, the place of true sum of the series can be taken by its asymptotic value, calculated with an appropriate prescription.

Given $c_n \equiv c_n(Q, Q)$, it is always possible to reinstate the full μ dependence and determine $c_n(Q, \mu)$ ([13] appendix A).

Since theoretical calculations for QCD cross section are known up to a perturbative order k , it is useful to define the partial sum as

$$\sigma_k(Q, \mu) \equiv \sum_{n=0}^k c_n(Q, \mu) \alpha_S^n(\mu), \quad (3.1.3)$$

(or $\sigma_k \equiv \sum_{n=0}^k c_n \alpha_S^n$ for $\mu = Q$) and the remainder of the series as

$$\Delta_k \equiv \sum_{n=k+1}^{\infty} c_n \alpha_S^n. \quad (3.1.4)$$

3.2 Scale variation

The most common way to estimate the effects of the unknown higher order contributions in QCD perturbative series is the scale variation method, which consists in studying the variation of the series with unphysical momentum scales. This variation usually involves the renormalisation scale μ_R , on which the strong coupling constant α_S depends, and the factorisation scale μ_F , at which one performs the matching between the perturbative calculation of the matrix elements and the non-perturbative part which resides in the parton distribution functions.

As already remarked above, the dependence on these scales is not physical: when all orders of the perturbative series are summed, the observables are scale independent. The reason why cross sections or distributions do depend on the scale is that they are truncated, as only their few first orders are evaluated in practice. This dependence can thus serve as a guess for the impact of the higher order contributions.

The start point for the momentum scale Q is usually considered as the most natural scale of the process, for instance the Higgs mass m_H in the case of Higgs production cross section. The current convention is to vary the two scales within the range (as discussed in [12])

$$\frac{Q}{\kappa} \leq \mu_R, \mu_F \leq \kappa Q, \quad (3.2.1)$$

with the constant factor κ to be determined. Then the deviation δ_k of a cross section $\sigma(\mu_R, \mu_F)$ from the central value evaluated at scales $\mu_R = \mu_F = Q$ is computed:

$$\sigma_k^+ = \max_{(\mu_R, \mu_F)} \sigma_k(Q, \mu_R, \mu_F), \quad (3.2.2)$$

$$\sigma_k^- = \min_{(\mu_R, \mu_F)} \sigma_k(Q, \mu_R, \mu_F), \quad (3.2.3)$$

$$\delta_k = \sigma_k^+ - \sigma_k^-. \quad (3.2.4)$$

The choice of the parameter κ is rather subjective, but it has become quite customary to fix $\kappa = 2$, even if much larger values are sometimes adopted, depending on the rate of convergence of the series.

Furthermore, there are several ways to treat the variation of the scales in the range of Equation (3.2.1). For example, μ_R and μ_F can be considered as independently varying in this domain, with possibly some constraints such as $1/\kappa \leq \mu_R/\mu_F \leq \kappa$ in order not to generate

artificially large logarithms. Otherwise, one of the two scales can be kept fixed, say to Q , letting the other scale vary in the chosen domain. Another possibility is to equate the two scales, $Q/\kappa \leq \mu_R = \mu_F \leq \kappa Q$.

The reason why this simple procedure can often work is that, under certain circumstances, the size of δ_k can be similar to the size of Δ_k . One can indeed show that ([13] appendix A)

$$\delta_k = \left. \frac{d\sigma}{d \ln \mu_R^2} \right|_{\mu_R=Q} [\ln(\kappa Q)^2 - \ln(Q/\kappa)^2] + \mathcal{O}(\ln^2 Q^2) \simeq 4 \ln \kappa k \beta_0 \alpha_S^{k+1} |c_k|. \quad (3.2.5)$$

Equality (3.2.5) is obtained by making the assumption that all the coefficients in the series share the same magnitude and that α_S is reasonably small. Under these same hypotheses (and therefore $|c_{k+1}| \simeq |c_k|$), the remainder of the series Δ_k can be approximated by the first unknown term, and hence δ_k :

$$|\Delta_k| \simeq \alpha_S^{k+1} |c_{k+1}| \sim \delta_k. \quad (3.2.6)$$

Tests with partially known perturbative calculations in QCD have shown that this kind of estimate for the theoretical uncertainty is reasonably successful in predicting the range in which a higher order result will fall. In spite of that, the limitation of this conventional approach is that, even if the hypothesis $|c_{k+1}| \simeq |c_k|$ is correct and therefore δ_k correctly describes the size of the remainder of the series², there is no way of determining with how much confidence it does so.

3.3 The Cacciari-Houdeau Method

The main shortcoming of the scale variation is that it does not provide the degree of belief of the resulting uncertainty bands. In other words, it does not associate a value to the probability that the uncertainty band contains the true sum of the series. This lack of a proper characterization makes it also difficult to combine theoretical uncertainties with other sources of uncertainties, like the value of α_S and the statistical uncertainty on PDFs discussed in Section 2.4. As a result, it appears to be impossible to rigorously assess the degree of belief that an experimental result may agree or not with theory and hence to confidently guess the discovery of new physics. The Cacciari-Houdeau Method [13] aims to provide theoretical uncertainty with a well defined credibility measure, so that the degree of belief of a given interval can be explicitly calculated.

To achieve this goal, the method makes use of the *Bayesian probability* (also called *subjective probability* or *degree of belief* or *credibility*), which needs to be distinguished from the *frequentist probability*. The two concepts share the same mathematical formalism, but are nonetheless distinct. Bayesian probability is not linked to an infinite number of realizations of an experiment. It deals with a particular question, which may or may not be about the result of one particular realization of a given experiment, and the consequences of the information one considers about its possible answer. This information is not necessarily rigorous or “true” in any way, but its treatment, once translated mathematically into the so called *priors* and *likelihoods*, is.

A distribution of frequentist probability (or, for instance, its variance) gives a measure of the reproducibility of an experiment. Conversely, a credibility distribution conveys information about the uncertainty of the answer to a question, such as the result of one particular realization

²As argued in Chapter 4, this approximation turns out to be inappropriate in the case of Higgs cross section. A possible solution to that is given in Section 4.4.

of an experiment, prior to its execution. The variables appearing in a frequentist probability distribution are commonly denoted as random variables, since they take different values in different realizations of the experiment. We call instead uncertain variables the ones in a credibility distribution, to better make the distinction with the former ones: their values are not random (each of them being a single number), but simply unknown.

Clearly, the uncertainties can only be interpreted in the latter sense: the true value is unique, and not random.

3.3.1 Model hypotheses

For what concerns a generic perturbative series, the uncertain variables are the a priori unknown coefficients c_0, c_1, \dots . A density function $f(c_0, c_1, \dots)$ is then defined over the space of the coefficients, whose constraints are normalization and the possibility of extracting one or more parameters:

$$\int f(c_0, c_1, \dots) dc_0 dc_1 \dots = 1, \quad (3.3.1)$$

$$f(c_0, \dots, c_{i-1}, c_{i+1}, \dots) = \int f(c_0, \dots, c_{i-1}, c_i, c_{i+1}, \dots) dc_i, \quad (3.3.2)$$

$$f(c_0, c_1, \dots, c_k) = \int f(c_0, c_1, \dots) dc_{k+1} dc_{k+2} \dots \quad (3.3.3)$$

Since the final target is to get information on the unknown remainder of the series Δ_k , given the first k known coefficients $f(\Delta_k | c_0, \dots, c_k)$, a conditional density needs to be introduced. For example, the density over the still unknown coefficient c_{k+1} , according to the standard rule, would read

$$f(c_{k+1} | c_0, \dots, c_k) = \frac{f(c_{k+1}, c_0, \dots, c_k)}{f(c_0, \dots, c_k)}. \quad (3.3.4)$$

The model rests then on the following four hypotheses:

Upper bound

The first assumption, coherent with the observations made for the scale variation in Section 3.2, is that successive perturbative coefficients of a series have similar magnitudes, so that they can all share some sort of upper bound $\bar{c} > 0$ to their absolute values, specific to the physical process studied. The known coefficients will then give an estimate of \bar{c} , restricting the possible values for the unknown coefficients c_n for $n > k$. Therefore, the set of uncertain variables that constitute the space on which the credibility measure is defined is made of this parameter \bar{c} and all of the unknown coefficients

Residual uncertainty

Another assumption is that, knowing the parameter \bar{c} in advance, the residual density for the value of an unknown coefficient is a uniform distribution,

$$f(c_n | \bar{c}) = \frac{1}{2\bar{c}} \chi_{|c_n| \leq \bar{c}}, \quad (3.3.5)$$

where χ_A is the characteristic function of a set A. It might be more appropriate to choose a density function that does not vanish anywhere, like a Gaussian distribution of mean zero

and standard deviation \bar{c} , but it can be shown that the general behaviour of the results is not significantly modified by this choice.

Shared information and independence

The parameter \bar{c} is required to be the only one that models information which is shared by all coefficients. As a result, as soon as \bar{c} is known, the residual uncertainties on the values of two coefficients c_n and c_m are totally independent, so that for a set of coefficients $\{c_i\}$ the joint density is simply the product of the marginal densities:

$$f(\{c_i\}, i \in I | \bar{c}) = \prod_{i \in I} f(c_i | \bar{c}). \quad (3.3.6)$$

The value of \bar{c} corresponds to the maximal knowledge that can be extracted from the known coefficients c_0, \dots, c_k in order to predict the possible values of the unknown ones.

Hidden parameter

The value of \bar{c} is “hidden” in the knowledge of the c_n : as long as none of the coefficients has been calculated, the only assumption we can make is that it is a positive real number, and that all values for its order of magnitude are equally probable. To implement this in practice a density for its logarithm is defined as the limit of a uniform distribution between $|\ln \epsilon|$ and $-|\ln \epsilon|$ for $\epsilon \rightarrow 0$:

$$f_\epsilon(\ln \bar{c}) = \frac{1}{2|\ln \epsilon|} \chi_{|\ln \bar{c}| \leq |\ln \epsilon|} \Leftrightarrow f_\epsilon(\bar{c}) = \frac{1}{2|\ln \epsilon|} \frac{1}{\bar{c}} \chi_{\epsilon \leq \bar{c} \leq 1/\epsilon}. \quad (3.3.7)$$

All the calculations which lead to the results in section 3.3.2 will be performed keeping $\epsilon \neq 0$ until the end, computing the limit $\epsilon \rightarrow 0$ afterwards. The vanishing of a density in this limit would mean that we do not have enough information to make any guess about the result.

These four hypotheses define completely the credibility measure over the whole space of a priori uncertain variables $\{c_0, c_1, \dots\}$. They also define every possible inherited measure on a subspace associated with a physical process whose the first k coefficients are known.

3.3.2 Model Outcomes

Let us consider now a perturbative series starting at $n = l$. Using the four hypotheses in Section 3.3.1, and defining $\bar{c}_{(k)} \equiv \max(|c_l|, \dots, |c_k|)$, the conditional density for the remainder Δ_k can be finally obtained (see [13] for a complete derivation):

$$f(\Delta_k | c_l, \dots, c_k) = \int \left[\delta \left(\Delta_k - \sum_{n=k+1}^{\infty} \alpha_S^n c_n \right) \right] f(c_{k+1}, c_{k+2}, \dots | c_l, \dots, c_k) dc_{k+1} dc_{k+2} \dots \quad (3.3.8)$$

This expression is too complicated to be handled analytically, even in the case of the simple choice of density in Equation (3.3.5) for the coefficients. However, making the approximation of Equation (3.2.6) which was valid for the scale variation method,

$$|\Delta_k| \simeq \alpha_S^{k+1} |c_{k+1}|, \quad (3.3.9)$$

and introducing the number of known coefficients $n_c = k + 1 - l$, one can obtain

$$f(\Delta_k | c_l, \dots, c_k) \simeq \left(\frac{n_c}{n_c + 1} \right) \frac{1}{2\alpha_S^{k+1} \bar{c}_{(k)}} \begin{cases} 1 & \text{if } |\Delta_k| \leq \alpha_S^{k+1} \bar{c}_{(k)} \\ \frac{1}{(|\Delta_k| / (\alpha_S^{k+1} \bar{c}_{(k)}))^{n_c + 1}} & \text{if } |\Delta_k| > \alpha_S^{k+1} \bar{c}_{(k)} \end{cases}. \quad (3.3.10)$$

This result depends on the entire set of the calculated coefficients via the parameter $\bar{c}_{(k)} = \max(|c_l|, \dots, |c_k|)$. The knowledge of $f(\Delta_k | c_l, \dots, c_k)$ allows one to calculate the smallest p -credible interval for Δ_k . Since it is centred at zero, it will be denoted by $[-d_k^{(p)}, d_k^{(p)}]$. It is defined implicitly by

$$p = \int_{-d_k^{(p)}}^{d_k^{(p)}} f(\Delta_k | c_l, \dots, c_k) d\Delta_k. \quad (3.3.11)$$

Finally, using the analytical approximation in Equation (3.3.10), it can be shown that

$$d_k^{(p)} = \begin{cases} \alpha_S^{k+1} \bar{c}_{(k)} \frac{n_c + 1}{n_c} p & \text{if } p \leq \frac{n_c}{n_c + 1} \\ \alpha_S^{k+1} \bar{c}_{(k)} [(n_c + 1)(1 - p)]^{-1/n_c} & \text{if } p > \frac{n_c}{n_c + 1} \end{cases}, \quad (3.3.12)$$

where, of course, $p \equiv P/100$ and P is a number between 0 and 100.

3.4 Example: PDFs

Now that we have a tool that allows us to assign a meaningful degree of belief to theoretical uncertainty estimates, we may want to try it on Parton Distribution Functions defined in Chapter 2. To do so, we make the assumption that PDFs are perturbative series in α_S :

$$f^{\text{LO}}(x) = c_0(x), \quad (3.4.1)$$

$$f^{\text{NLO}}(x) = f^{\text{LO}}(x) + c_1(x) \alpha_S, \quad (3.4.2)$$

$$f^{\text{NNLO}}(x) = f^{\text{NLO}}(x) + c_2(x) \alpha_S^2, \quad (3.4.3)$$

where $f(x)$ is a generic PDF. Since the LHAPDF interface provides parton distributions to any order for each flavour, once the coefficients c_0, c_1, c_2 are computed, Equation 3.3.12 can be used to derive the p credible uncertainty interval around the k order value. In the next plots Cacciari-Houdeau 1σ (68.27%) relative uncertainties (i.e. divided by the PDF values) are plotted, together with the relative statistical uncertainties and, when possible, with the relative difference between the next-order and the current-order exact value. All flavours have been studied at $Q = 100$ GeV and for $\alpha_S(M_Z) = 0.118$. The Gluon PDF in particular, obtained with NNPDF 2.3 and MSTW2008, is shown and discussed in more detail, as an example for all the other flavours.

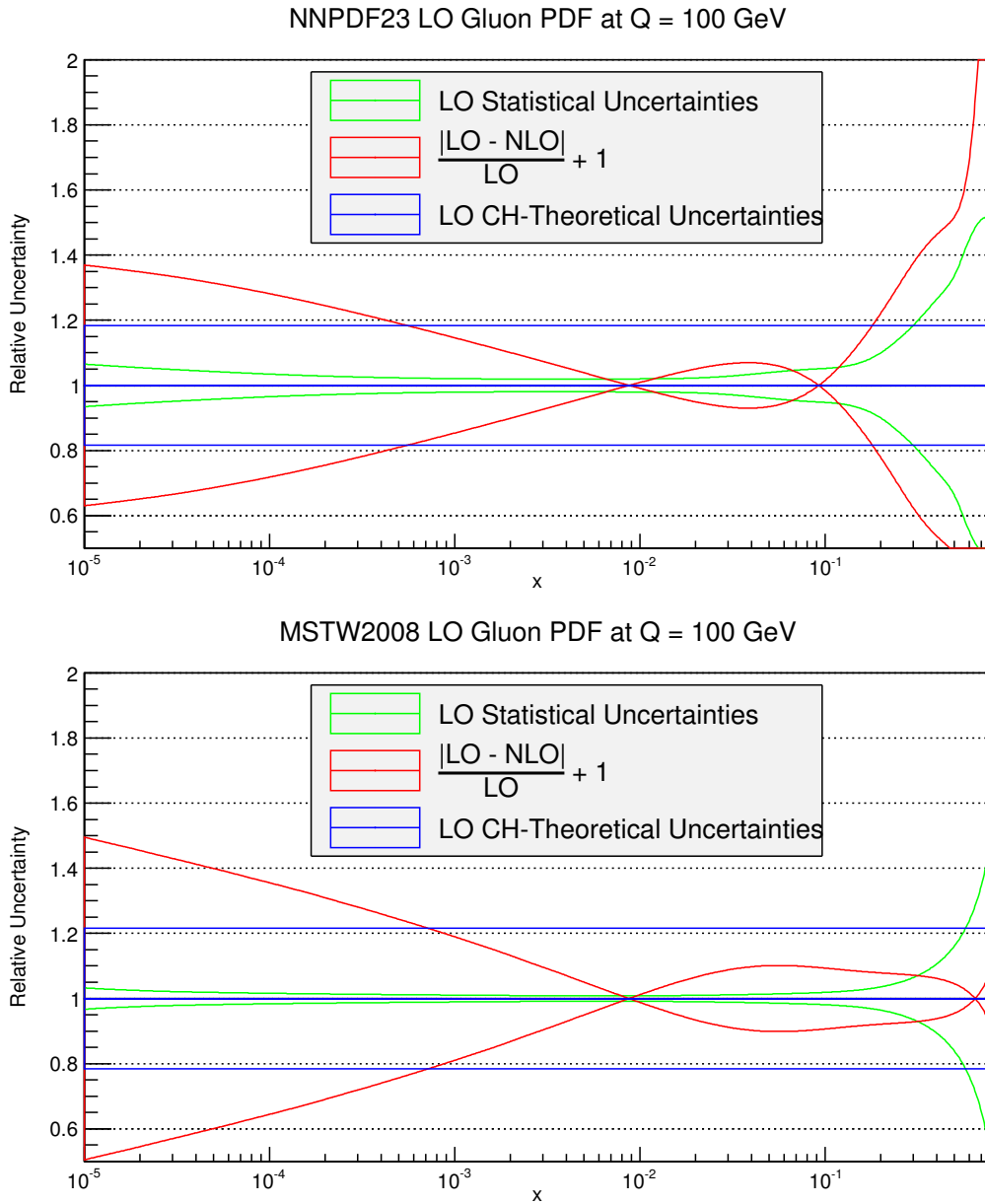


Figure 3.1: LO uncertainties on gluon PDF.

3.4.1 Leading Order

At LO the theoretical uncertainty can only be fixed, as $\bar{c}_{(k)}(x) \equiv c_0(x)$, and from Equation in 3.3.12 we can see that dividing by $f^{\text{LO}}(x) = \bar{c}_{(k)}(x)$ it ends up being proportional to α_S , which is constant because $Q = 100$ GeV. Even if computing the Cacciari-Houdeau theoretical uncertainty with only one known coefficient might not seem a sensible way to proceed, the next-order (NLO) lies within the LO uncertainty band for most of the x interval considered. Theoretical uncertainty is at this level much higher than statistical uncertainty, meaning that the error which comes from error propagation during the PDF extraction can be neglected in comparison to the uncertainty arising from higher terms in the perturbative series.

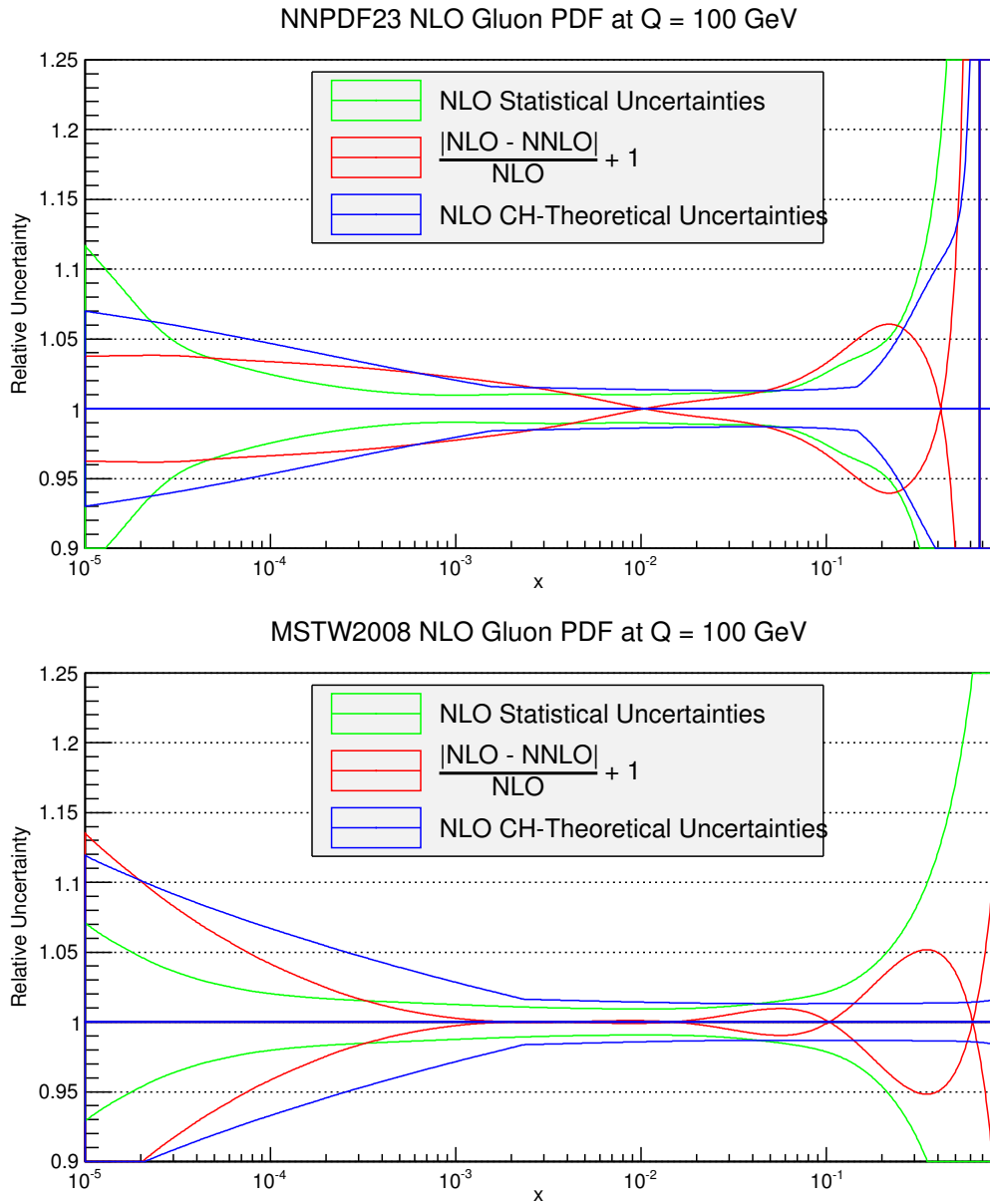


Figure 3.2: NLO uncertainties on gluon PDF.

3.4.2 Next to Leading Order

With two coefficients available, the NLO theoretical uncertainty is not flat anymore. The NNLO PDF stays completely inside the C-H interval, as the red line in Figure 3.2 lies almost always below the blue one. Furthermore, theoretical and statistical uncertainties are now of the same size, as one might have expected.

In fact, there is no reason for the relative statistical uncertainty to significantly change with the perturbative order, since its computation, as described in Section 2.4, only reflects error propagation of experimental data. Theoretical uncertainty, instead, varies with the order, and in particular it should decrease with increasing perturbative orders if the perturbative expansion converges (strictly or asymptotically)

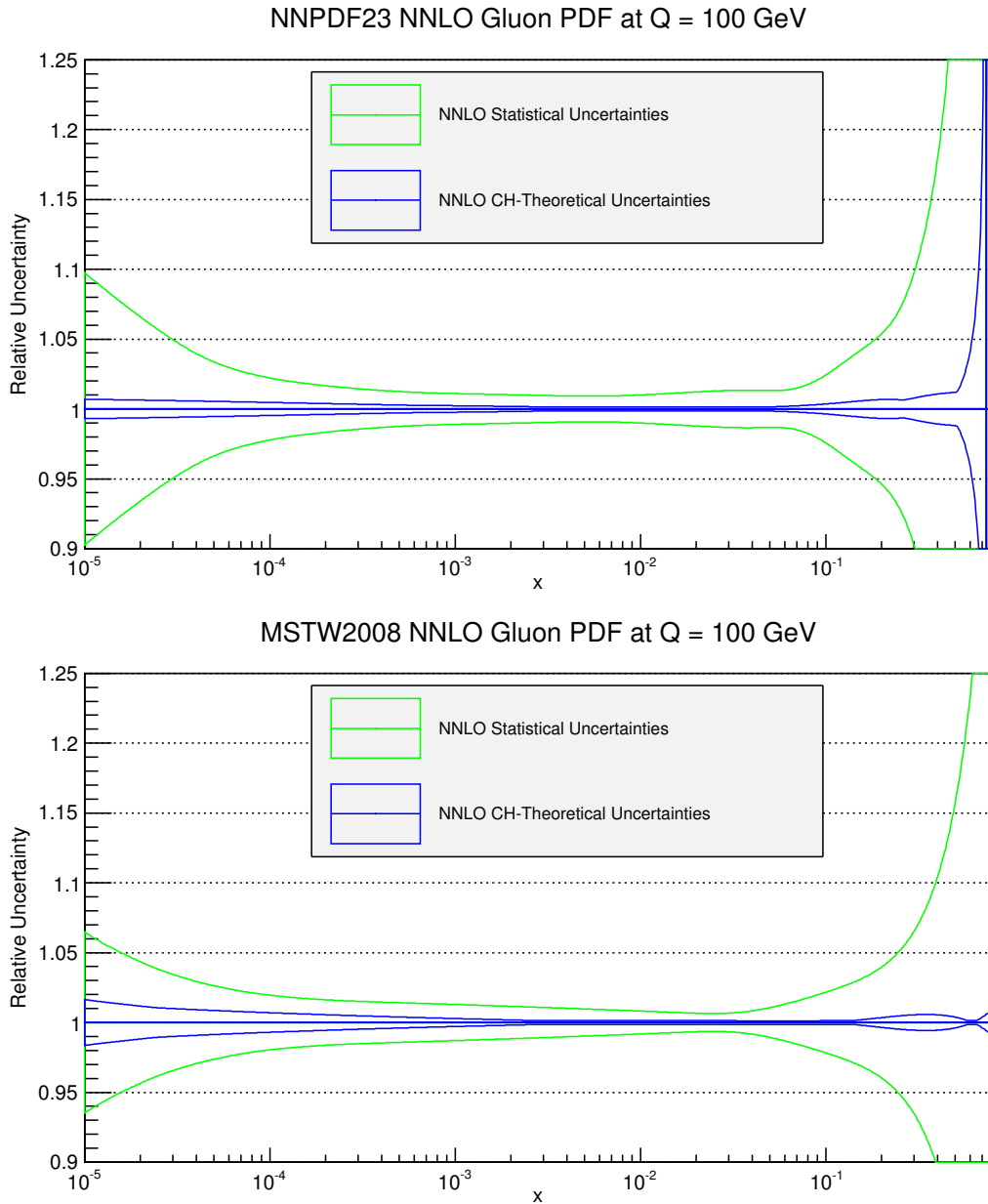


Figure 3.3: NNLO uncertainties on gluon PDF.

3.4.3 Next to Next to Leading Order

As anticipated in Section 3.4.2, the theoretical uncertainty decreases as the perturbative order increases, until at NNLO it becomes much smaller than the statistical uncertainty. Since $N^3\text{LO}$ PDFs do not exist, there is no way of checking their compatibility with the 1σ C-H NNLO uncertainty interval. However, if all the assumptions made in Section 3.3.1 are sensible, it is possible now to quantify how much would PDFs change if there was a $N^3\text{LO}$ PDF set: up to a maximum of $\sim 0.1\%$ for reasonable values of x . For completeness, in Figure 3.4 and 3.5 NLO plots are delivered for all flavours (top excluded because too heavy for $Q = 100$ GeV) in both logarithmic and linear scale.

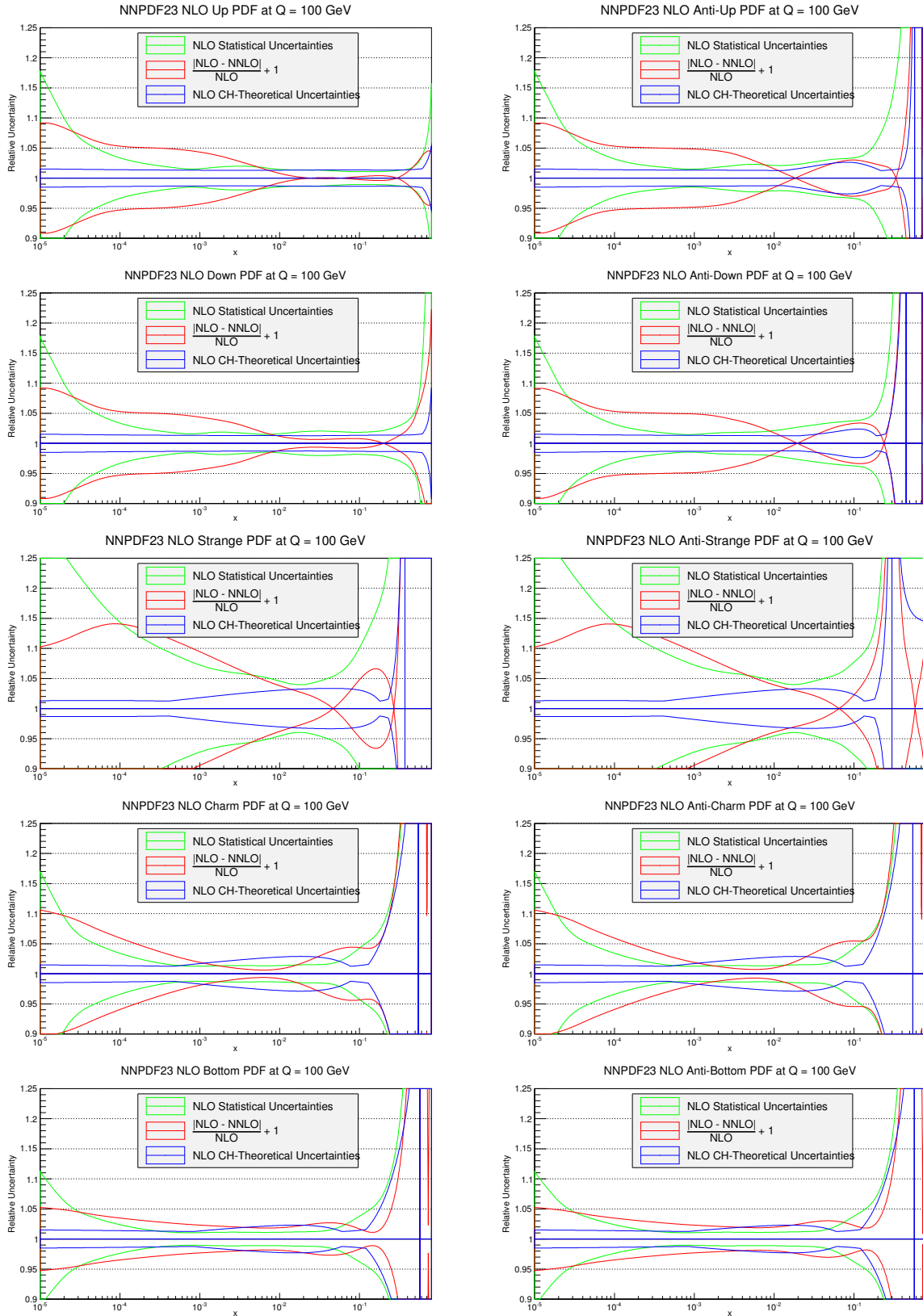


Figure 3.4: NLO uncertainties on PDFs (NNPDF 2.3) of all flavours in logarithmic scale.

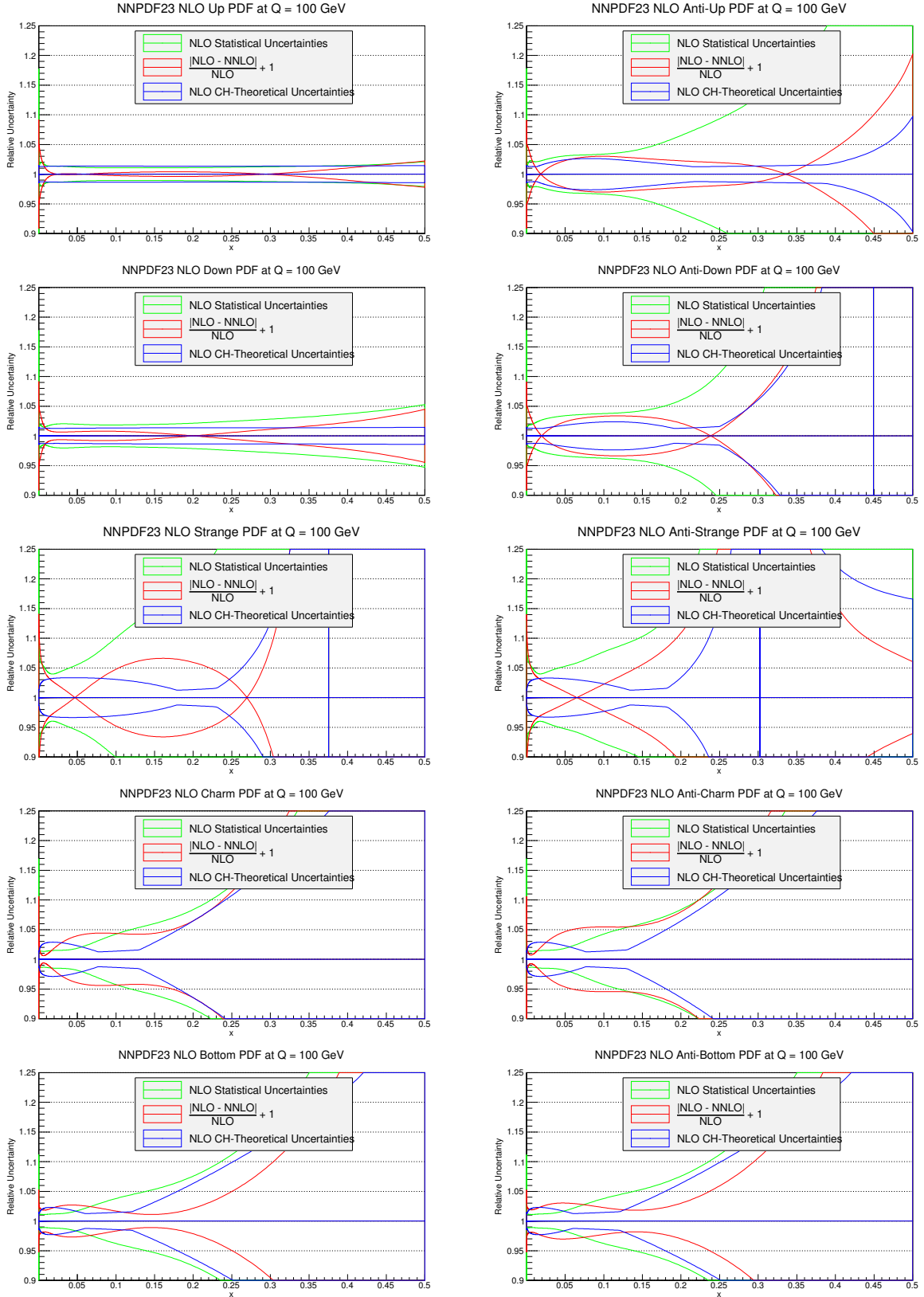


Figure 3.5: NLO uncertainties on PDFs (NNPDF 2.3) of all flavours in linear scale.

3.4.4 Choice of the expansion parameter α_S

In Equations 3.4.2 and 3.4.3, as well as in the Cacciari-Houdeau final formula 3.3.12, we make use of the strong coupling α_S . Actually, α_S is not a constant, but rather it depends on the energy Q and it evolves through the DGLAP perturbative equations.

There are several possible choices for $\alpha_S(Q)$ evolution: one could decide, for example, to let the strong coupling evolve at the same order as the PDF considered, so that the computation of theoretical uncertainty and of the c_n coefficients would be performed with an α_S which evolves consistently with PDFs and with the way PDF themselves are determined.

However, in this work the decision is made to let always α_S evolve according to the NNLO DGLAP equations. By considering the highest known perturbative order of the DGLAP equation, it is as if we were always taking the “best” value for α_S . This choice will also be made in Section 3.5 and in Chapter 4

3.4.5 Impact of Statistical Uncertainty

Except for the gluon PDF, which seems to behave very well, the quark PDFs in Figure 3.4 have a $|\text{NNLO} - \text{NLO}|$ shift that is, at low x , larger than the theoretical uncertainty bands. The straightforward explanation is that, especially for quarks, the region where most of the data for PDF determination are available is around from $\sim 10^{-2}$ to ~ 0.5 . Within this range, the NNLO PDFs do stay inside the $\text{NLO} + 1\sigma$ bands in almost every case. Away from this region, though, statistical uncertainties become so large that the mean can fluctuate wildly, so that the NNLO PDF can be extremely different from the NLO due to statistical fluctuations.

3.5 Example: Parton Luminosities

The results of Section 3.4 give a first indication, but they are not sufficient for a study of the impact of PDF uncertainty onto the Higgs Cross Section. In fact, the relation between a parton distribution and a hard cross section is slightly more complicated.

3.5.1 Definition

Starting from equation (2.3.2), one can write

$$\sigma_X(s, M_X^2) = \sum_{a,b} \sigma_{ab}^0 \int_{\tau}^1 \frac{dx}{x} \mathcal{L}_{ab}(M_X^2) C_{ab}\left(\frac{\tau}{x}, \alpha_S(M_X^2)\right), \quad (3.5.1)$$

where a parton luminosity $\mathcal{L}_{ab}(M_X^2)$ between two PDFs of quarks a, b is defined as the following convolution integral, with τ defined in Equation (2.3.3):

$$\mathcal{L}_{ab}(M_X^2) \equiv \frac{1}{s} \int_{\tau}^1 \frac{dx}{x} f_{a/h_1}(x, M_X^2) f_{b/h_2}\left(\frac{\tau}{x}, M_X^2\right). \quad (3.5.2)$$

Now, the parton luminosity depends solely on two PDFs, while the hard coefficient functions C_{ab} depend on the partonic cross sections specific of the process considered. Consequently, studying theoretical uncertainties on luminosities is a first step towards the isolation of the PDF dependence of an inclusive cross section. However, a QCD cross section, for instance Higgs production at LHC, usually depends on more than one luminosity. In our case, gluon fusion is by far the dominant channel, so that we are mostly interested in the gluon-gluon luminosity.

3.5.2 Perturbative series

Once again, we have to clarify in what sense parton luminosities are perturbative series in α_S . We assume that the perturbative order of a luminosity corresponds to that of the PDFs of which it is made of³:

$$\mathcal{L}_{ab}^{\text{LO}} = f_a^{\text{LO}} \otimes f_b^{\text{LO}}, \quad (3.5.3)$$

$$\mathcal{L}_{ab}^{\text{NLO}} = f_a^{\text{NLO}} \otimes f_b^{\text{NLO}}, \quad (3.5.4)$$

$$\mathcal{L}_{ab}^{\text{NNLO}} = f_a^{\text{NNLO}} \otimes f_b^{\text{NNLO}}, \quad (3.5.5)$$

where we denoted with \otimes the convolution integral of Equation (3.5.2).

With this expression of the luminosity, we are including some interference terms, i.e. higher order terms such as $c_{1,a} c_{1,b} \alpha_S^2$ at NLO and $c_{1,a} c_{2,b} \alpha_S^3 + c_{2,a} c_{1,b} \alpha_S^3 + c_{2,a} c_{2,b} \alpha_S^4$ at NNLO. However, these terms are perturbatively subleading.

3.5.3 Results for M_X

Considerations on theoretical uncertainties on luminosities are exactly the same for PDFs, with the only difference that luminosities are more conveniently expressed as functions of M_X^2 or, better, $\sqrt{\hat{s}}$, the center of mass energy of the partonic collision, instead of the Bjorken scaling x . Accordingly, they are point by point a perturbative series in $\alpha_S(M_X^2)$. That is the reason why, for example, LO theoretical uncertainty is not a flat function. In Figure 3.6 gluon-gluon luminosities at $\sqrt{s} = 8$ TeV for $\alpha_S(M_Z) = 0.118$ are plotted.

Again, the theoretical Cacciari-Houdeau uncertainty is seen to generally decrease for increasing perturbative order, whereas statistical uncertainty remains almost completely unchanged in shape. The statistical uncertainty is computed⁴ according to equations (2.4.1), (2.4.2), (2.4.3) and (2.4.4), being the luminosity a function of the PDFs.

The MSTW set seems to present an unrealistically small shift between NLO and NNLO. This may be perhaps due to a bias in MSTW PDF determination, which causes NLO to be almost equal to NNLO, and hence the relative shift to be close to zero.

A Monte Carlo set like NNPDF, instead, is able to reproduce the effect of the raising statistical uncertainty at high $\sqrt{\hat{s}}$ with a consistent increase the shift. The reason why this happens is that M_X is proportional to $\tau = M_X/s$, so that in the integral of Equation 3.5.2 higher x contributions become dominant at large M_X , making experimental uncertainties more relevant.

3.5.4 Results for $M_X = m_H$

A specific value of M_X is taken into account for the gluon-gluon luminosity: the Higgs mass. Figure 3.7 shows the trend of theoretical Cacciari-Houdeau 1σ uncertainties in gluon-gluon luminosity at $\sqrt{\hat{s}} = m_H$, while Tables 3.1 and 3.2 present numerical values (multiplied by 10^3) together with percent errors and absolute errors.

Looking at the coefficients c_n , it is also possible to verify a posteriori the validity of our first hypothesis, namely that they share the same magnitude. The column *Shift* indicates the absolute value of the difference between luminosity computed at successive orders, namely $|\mathcal{L}^{(k)} - \mathcal{L}^{(k+1)}|$. If it is found to be smaller than the error band, it is marked with a ✓ in the column *Match*.

³From now on the trivial M_X^2 dependence shall be neglected.

⁴Through a standalone code available on [15].

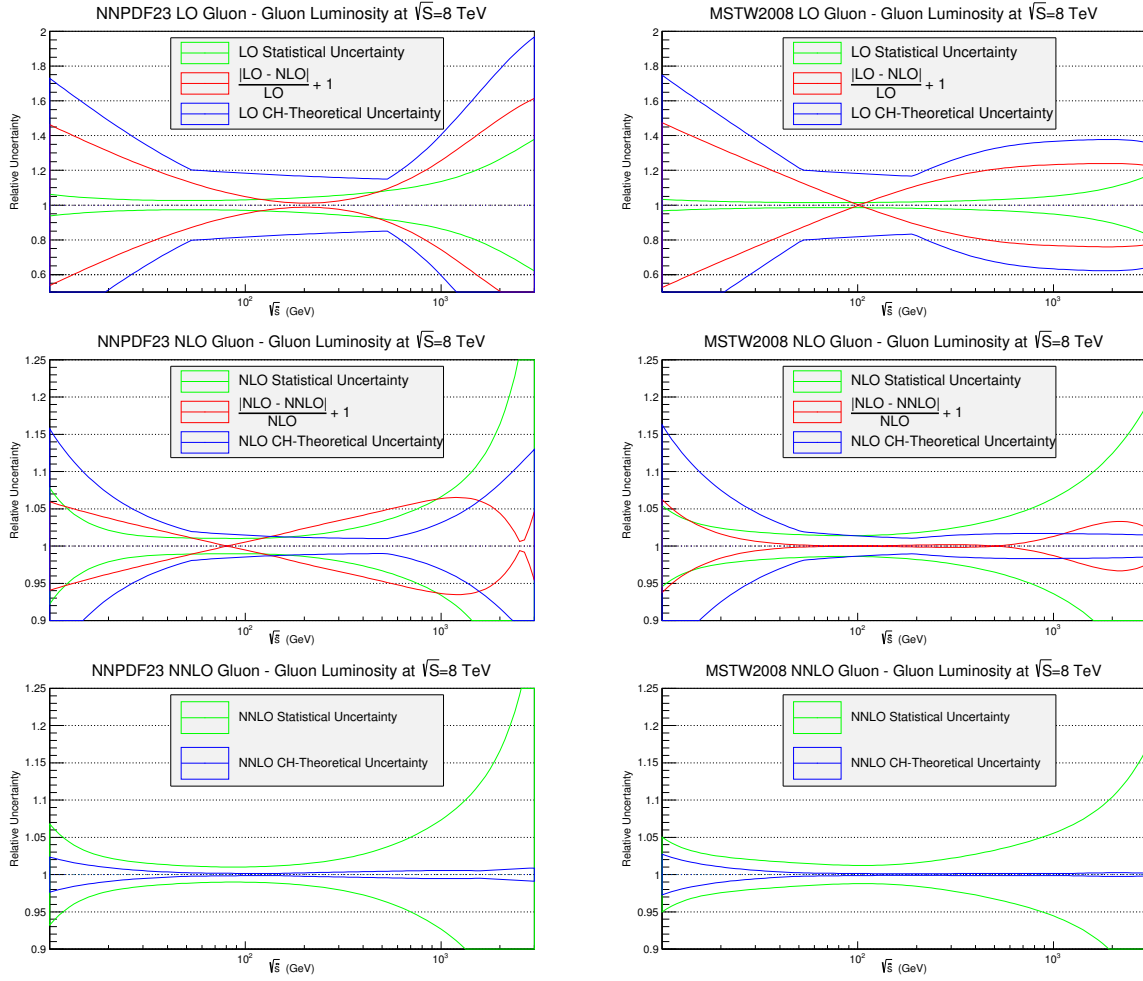


Figure 3.6: Gluon-gluon luminosity at $\sqrt{s} = 8$ TeV for both NNPDF23 and MSTW2008.

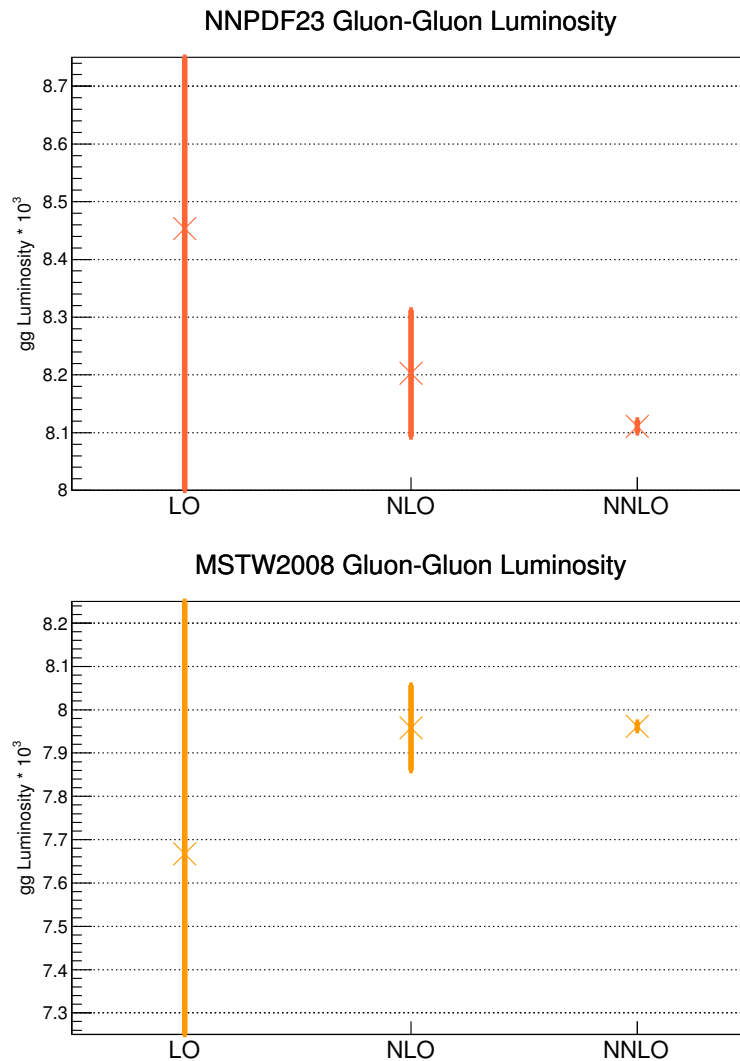
So far, a new model for theoretical uncertainty estimates has been introduced and tested on PDFs and on gluon-gluon luminosity. The next step involves studying the cross section for Higgs production, analysing theoretical uncertainties and, possibly, separating the PDF contribution from that of the cross section itself. According to Equation (2.3.1) we expect the PDF contribution to have a similar trend to that of gluon-gluon luminosity, being gluon fusion the dominant channel in Higgs production.

Table 3.1: **NNPDF2.3** $\alpha_S(m_Z) = 0.118$ gluon-gluon luminosity at m_H .

\mathcal{L}	Val	c_n	Error(%)	Error	Shift	Match
LO	8.45359	8.45359	17.735%	1.49924	0.250997	✓
NLO	8.2026	-2.2301	1.33806%	0.109756	0.0916264	✓
NNLO	8.11097	-7.23321	0.135259%	0.0109708		

Table 3.2: **MSTW2008** gluon-gluon luminosity at m_H .

\mathcal{L}	Val	c_n	Error(%)	Error	Shift	Match
LO	7.66734	7.66734	17.6016%	1.34957	0.290847	✓
NLO	7.95819	2.60375	1.23214%	0.0980557	0.00365731	✓
NNLO	7.96185	0.293111	0.122177%	0.00972754		

Figure 3.7: Gluon-Gluon luminosity series at $M_X = m_H$ for both NNPDF 2.3 and MSTW2008.

Chapter 4

Theoretical Uncertainties on Higgs Cross Section

Armed with a tool capable of assigning a meaningful degree of belief to theoretical uncertainty estimates, we can now test it on the Higgs production cross section. Predictions for the series are obtained through the use of two codes: `ggHiggs` [16] and `iHixs` [17], each of which performs calculations on any required PDF set. After having checked that the two results are in good agreement, either of them could be used in principle, but the former is preferred as it also provides an approximate N³LO cross section.

The PDF impact on the cross section is then isolated and analysed. The reason why this is important is that, although the exact N³LO Higgs cross section will soon be available, a N³LO for splitting functions, and thus N³LO parton distributions are unlikely to be available in the forthcoming future. So, a crucial issue is whether or not it is reasonable to use NNLO PDF sets to compute N³LO cross section, and what could the effects be on the final result. If the PDF contribution to the theoretical uncertainty at the highest known order is negligible, then a N³LO PDF is not urgently required.

After that, the NNLO PDF set is selected and the perturbative cross section examined. The pure Cacciari-Houdeau method turns out to be insufficient in order to estimate the remainder of the series, as the most important model hypothesis is manifestly violated. So, a modified version of the model is introduced where the expansion parameter does not necessarily have to be α_S . The choice of the new parameter will lead in Section 4.4 to interesting considerations on the structure of the series itself.

Then, the outcomes of this new model are compared and contrasted to those of the standard scale variation method, so as to provide another proof of the validity of the former.

Finally, in order to determine the effective PDF influence, its uncertainty needs to be compared with the theoretical uncertainty which only arises from the perturbative nature of the partonic cross sections, at a fixed PDF. This comparison will eventually determinate the impact of theoretical uncertainties on PDFs on the Higgs cross section.

4.1 `ggHiggs` and `iHixs`

The two codes are able to compute the cross section for the inclusive Higgs production at hadron colliders, with full top mass dependence.

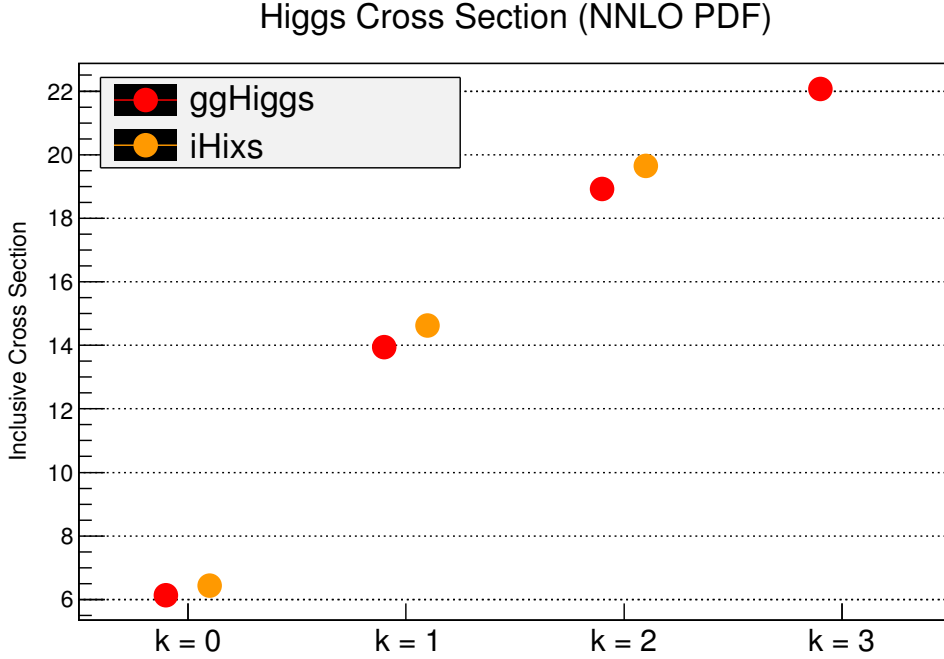


Figure 4.1: Comparison between ggHiggs and iHixs using the NNLO PDF.

- **iHixs** incorporates QCD corrections through NNLO, real and virtual electroweak corrections, mixed QCD-electroweak corrections, quark-mass effects through NLO in QCD, and finite width effects for the Higgs boson and heavy quarks [17].
- **ggHiggs** can compute the $N^3\text{LO}$ using an approximation based on a combination of optimized soft-collinear and high-energy behaviours [16].

Before any consideration on theoretical uncertainties we check that, once we use the same PDF set for both, results are consistent. Tests have been made for many sets at all orders and they all indicate the same good agreement. Actually, iHixs cross section is always found to be slightly larger than ggHiggs, but the differences compensate when computing the coefficients c_n . The plot in Figure 4.1 compares the cross sections obtained by the two programs using the NNLO PDF¹.

In order to avoid confusion, from now on k shall denote the order of a perturbative series σ_k like that of Equation (3.1.2), while LO, NLO and NNLO will indicate the orders of the PDF set used for its computation.

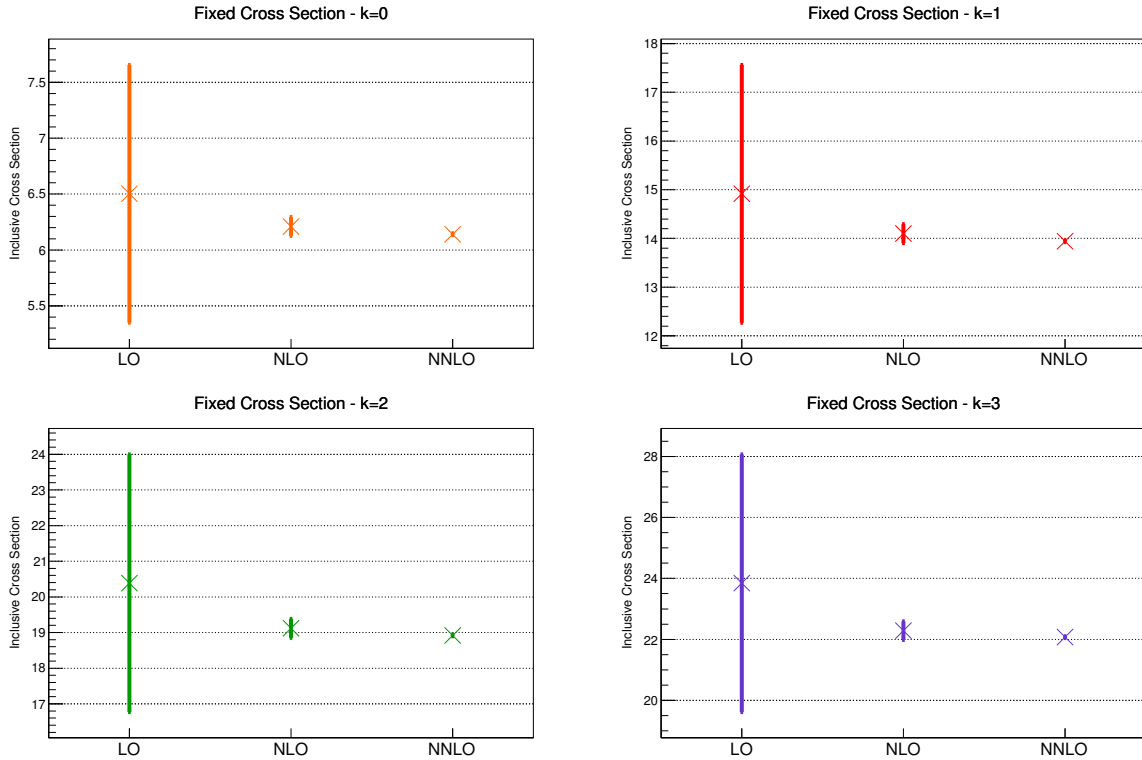
4.2 Fixed Cross Section

In Section 3.5 it was claimed that theoretical uncertainties on gluon-gluon luminosity at m_H should represent a good estimate of the impact of theoretical uncertainties on PDFs on Higgs cross section. However, gluon-gluon, though dominant, is not the only luminosity involved in the perturbative calculations. In order to completely isolate the PDF dependence, a possible

¹From now on only the NNPDF 2.3 $\alpha_S = 0.118$ shall be used.

Table 4.1: Results at fixed Cross Section for $0 \leq k \leq 3$.

k = 0						
PDF	Val	c_n	Error(%)	Error	Shift	Match
LO	6.39913	6.39913	17.735%	1.13488	0.189493	✓
NLO	6.20964	-1.68364	1.33796%	0.0830822	0.069221	✓
NNLO	6.14041	-5.46447	0.135245%	0.00830458		
k = 1						
PDF	Val	c_n	Error(%)	Error	Shift	Match
LO	14.6134	14.6134	17.735%	2.59169	0.514332	✓
NLO	14.0991	-4.56981	1.3457%	0.189731	0.154298	✓
NNLO	13.9448	-12.1807	0.135999%	0.0189648		
k = 2						
PDF	Val	c_n	Error(%)	Error	Shift	Match
LO	19.9084	19.9084	17.735%	3.53076	0.791253	✓
NLO	19.1172	-7.03025	1.35207%	0.258478	0.198223	✓
NNLO	18.919	-15.6482	0.136564%	0.0258365		
k = 3						
PDF	Val	c_n	Error(%)	Error	Shift	Match
LO	23.2317	23.2317	17.735%	4.12013	0.944764	✓
NLO	22.2869	-8.39419	1.35337%	0.301625	0.214529	✓
NNLO	22.0724	-16.9354	0.136593%	0.0301493		

Figure 4.2: Fixed Cross Section for $0 \leq k \leq 3$.

way to proceed is to look at how the cross section at a fixed k changes with the order of the PDF set.

This way, since the partonic cross section $\hat{\sigma}$ at a given k is constant, the three terms obtained by varying the PDF order only differ due to the effects of the PDF sets, see Equation (2.3.1). If these terms are now viewed as a perturbative series in α_S starting at $l = 0$, theoretical uncertainties on this series represent without any doubt the isolated impact of the PDFs on the Higgs cross section. In practice, we define

$$\sigma^{\text{LO}}|_{k=\text{cost}} = c_0, \quad (4.2.1)$$

$$\sigma^{\text{NLO}}|_{k=\text{cost}} = c_0 + c_1 \alpha_S, \quad (4.2.2)$$

$$\sigma^{\text{NNLO}}|_{k=\text{cost}} = c_0 + c_1 \alpha_S + c_2 \alpha_S^2, \quad (4.2.3)$$

where, as discussed in Section 3.4.4, α_S is always assumed to evolve at NNLO.

The computation of theoretical uncertainties is again performed using Equation (3.3.12), and the results for the NNPDF 2.3 set are plotted in Figure 4.2. As expected, the global shape is observed not to change much with k , as it reflects the influence of the PDF, which is independent of the cross section order. Furthermore, the plot is similar to that of the gluon-gluon luminosity in Figure 3.7, meaning that our assumption at the very end of Chapter 3 was well founded. In Table 4.1 numerical results are given, proving that the model prediction on known orders are well satisfied.

Looking at the results, the question raised at the beginning of this Chapter might be better understood, namely if and how it is wise to compute N³LO cross sections with NNLO PDF set. As a matter of fact, the PDF contribution to the Higgs cross section theoretical uncertainty at the last known PDF order is $\approx 0.1366\%$. This is the uncertainty that needs to be taken into account when performing such a computation. This is a small correction, however the relevant question is how small it is in comparison to the uncertainty on the cross section itself.

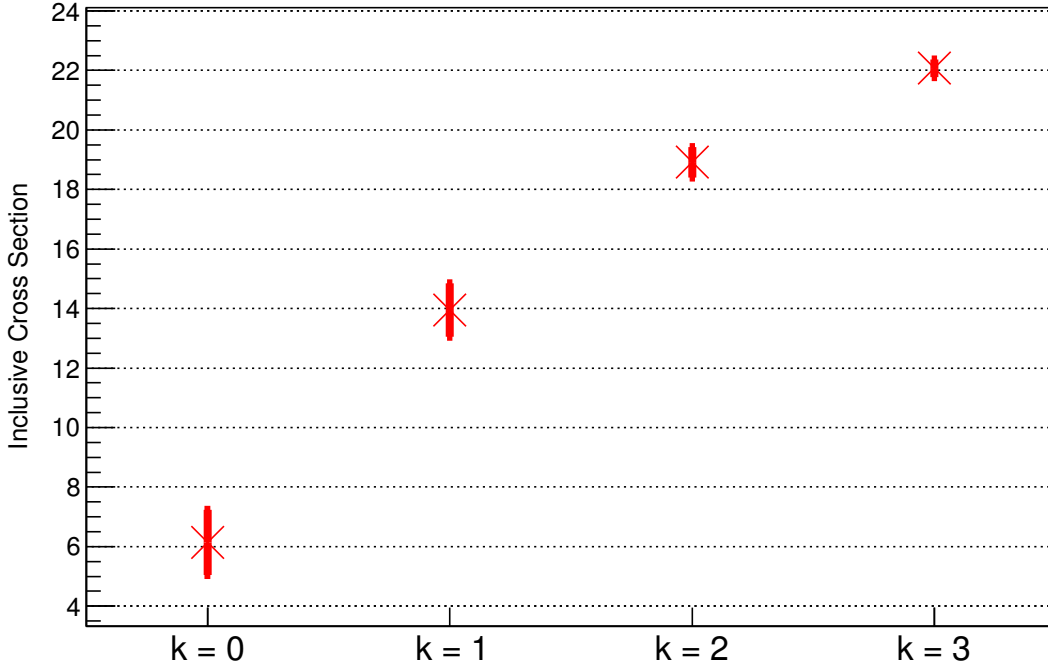
4.3 Fixed PDF

Now that the PDF impact has been computed, we can focus on the proper Higgs production cross section: a PDF set is chosen and theoretical uncertainties on σ_k are determined. Unfortunately, by naively applying the Cacciari-Houdeau formula (3.3.12) one gets an undesirable result. As shown in Figure 4.3, C-H intervals do not include the following order and, a fortiori, they are not capable of reliably predict the remainder of the series Δ_k .

Jumping to hasty conclusions, one may think that this proves that the model is inefficient or not suitable for this kind of perturbative series. Nevertheless, the reason of this apparent failure is soon explained when looking at Table 4.2. We have seen in Section 3.3.1 that the hypothesis on which the whole approach relies is that the coefficients c_n are all more or less of the same size, but for the Higgs production cross section this is evidently false, as the coefficients seem to gain a factor of almost 10 at each order. If we rejected that hypothesis in the first place, however, Equation (3.2.6) would not stand anymore, the remainder of the series Δ_k could not be approximated to the first unknown term $c_{k+1} \alpha_S^{k+1}$ and the density (3.3.4) would be of little help. However, we may question on the choice of the perturbative parameter.

Table 4.2: Fixed PDF results for $l = 0$, expansion parameter α_S .

LO PDF						
k	Val	c_n	Error(%)	Error	Shift	Match
0	6.39913	6.39913	17.735%	1.13488	8.2143	X
1	14.6134	72.9837	6.48426%	0.947573	5.29501	X
2	19.9084	418.001	2.72481%	0.542467	3.32322	X
3	23.2317	2330.91	1.37391%	0.319182		
NLO PDF						
k	Val	c_n	Error(%)	Error	Shift	Match
0	6.20964	6.20964	17.735%	1.10128	7.88946	X
1	14.0991	70.0975	6.45503%	0.910101	5.01809	X
2	19.1172	396.14	2.68919%	0.514097	3.16971	X
3	22.2869	2223.23	1.36599%	0.304437		
NNLO PDF						
k	Val	c_n	Error(%)	Error	Shift	Match
0	6.14041	6.14041	17.735%	1.089	7.80439	X
1	13.9448	69.3416	6.45607%	0.900287	4.97416	X
2	18.919	392.672	2.69358%	0.509597	3.15341	X
3	22.0724	2211.8	1.37217%	0.302871		

Fixed PDFs (NNLO) - $l = 0$ Figure 4.3: Cross Section with NNLO PDF for $l = 0$, expansion parameter α_S .

4.4 The parameter λ

So far, every perturbative series has been treated assuming the expansion parameter to be α_S , the natural parameter in QCD calculations. Still, we may rewrite Equation (3.1.2) as

$$\sigma_k = \sum_{n=l}^k c_n \alpha_S^n = \sum_{n=l}^k \frac{c_n}{\lambda^n} (\lambda \alpha_S)^n, \quad (4.4.1)$$

where l is again the starting order. This corresponds to a redefinition of the coefficients c_n into

$$c'_n = \frac{c_n}{\lambda^n}. \quad (4.4.2)$$

But how do we choose λ ? In principle, there may be theoretical arguments which suggest that the natural parameter differs from α_S by a constant, such as $\frac{\alpha_S}{2\pi}$. Lacking such an argument, we determine λ by the requirement that we will eventually get coefficients c'_n all of the same size.

The easiest way to do so is a fit to a distribution where $c'_n = \kappa \forall n$, with κ constant. Specifically, a two parameter fit is performed with ROOT in order to extract κ and λ from the known c_n of Equation (3.1.2), by demanding that

$$c_n = \kappa \lambda^n. \quad (4.4.3)$$

The λ thus obtained is then substituted into Equation (4.4.2), in order to determine the coefficients c'_n , because, even if they were all supposed to be $= \kappa$, it is reasonable to expect some fluctuations due to errors within the fitting procedure.

Figure 4.4 shows a logarithmic plot of the coefficients c_n together with the best fit function, while Table 4.3 displays numerical results for λ , their uncertainty due to the fit, and the goodness-of-fit χ^2 , for all the PDF sets. Surprisingly, the fit is found to be extremely accurate, as if the c_n were originally distributed according to Equation (4.4.3). In spite of that, the errors on λ are almost ten times larger than λ . As it can be seen from the plot, this is due to the fact that c_0 is quite different from the value predicted by the fit.

The λ extracted from the fit can be now used to compute theoretical uncertainties by placing $\lambda \alpha_S$ instead of α_S in Equation (3.3.12). The results, shown in Table 4.5 and Figure 4.3, are encouraging, since the shift is actually of the same size as the uncertainty band, which is found to be $\approx 7.75\%$ for $k = 3$ and NNLO PDF, about 50 times larger than the contribution coming from PDF theoretical uncertainties.

4.5 Series starting at $l = 1$

The parameter λ extracted in Section 4.4 provides satisfactory estimates for theoretical uncertainties. However, we have seen that the hypothesis that all coefficients follow Equation (4.4.3) is not well satisfied by c_0 . We may thus make the weaker assumption that

$$\sigma_k = \sigma_0(1 + \tilde{\sigma}_k), \quad \tilde{\sigma}_k = \sum_{n=1}^k d_n \alpha_S^n = \sum_{n=1}^k d'_n (\lambda \alpha_S)^n, \quad (4.5.1)$$

where all d_n are of similar order, but not of order 1.

This hypothesis is much better satisfied: the value of λ does not change much from Table 4.3, but the error decreases by a factor of $\sim 10^4$ and the χ^2 is about ten times smaller. One may wonder how this behaviour of the coefficients depends on μ_R . It turns out that if one plots the χ^2 of the coefficient fit at different μ_R , it has a manifest minimum at $\approx 0.995 m_H$, Fig 4.6. Table 4.6 and Figure 4.7 show theoretical uncertainty estimates for $\tilde{\sigma}_k$ when $\lambda = 1$.

Table 4.3: λ values for σ_k , $l = 0$.

PDF	λ	Error	χ^2
LO	5.59287	51.8111	0.0649917
NLO	5.62215	40.2395	0.0607445
NNLO	5.64197	38.5645	0.0602181

Table 4.4: λ values for $\tilde{\sigma}_k$, $l = 1$.

PDF	λ	Error	χ^2
LO	5.58483	0.084437	0.0238018
NLO	5.61446	0.00546015	0.00622921
NNLO	5.63439	0.00324891	0.00481135

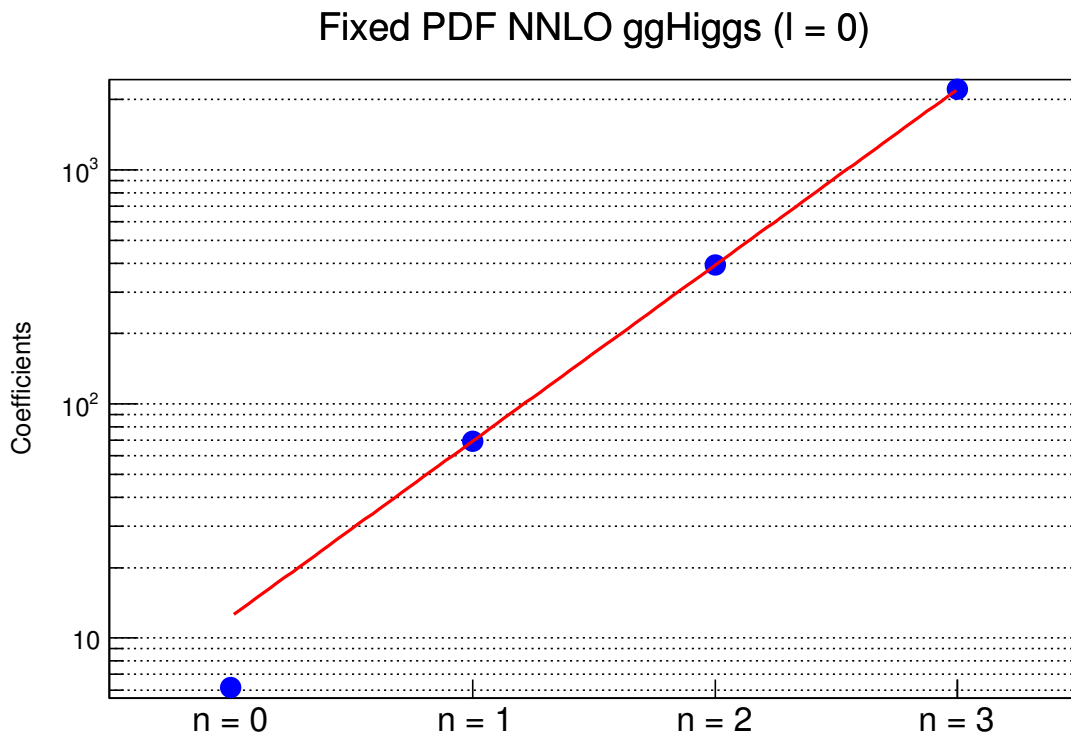
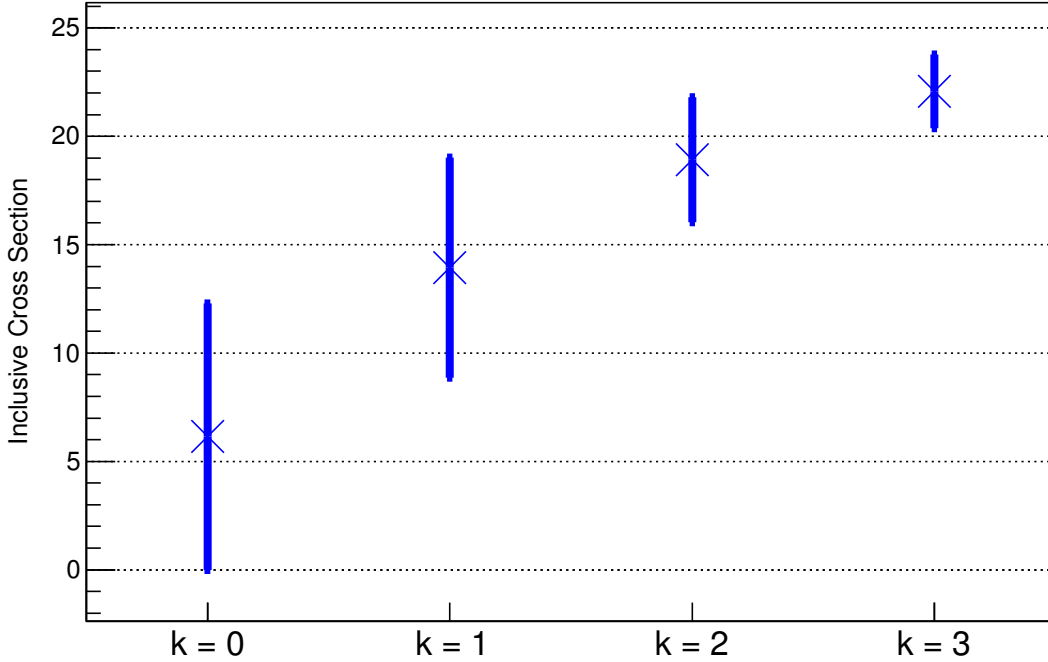
Figure 4.4: Coefficients c_n fitted as $\kappa \lambda^n$.

Table 4.5: Fixed PDF results for $l = 0$, expansion parameter $\lambda\alpha_S$.

LO PDF						
k	Val	c'_n	Error(%)	Error	Shift	Match
0	6.39913	6.39913	99.1894%	6.34726	8.2143	✗
1	14.6134	13.0494	36.2657%	5.29966	5.29501	✓
2	19.9084	13.3631	15.2395%	3.03395	3.32322	✗
3	23.2317	13.3235	7.70689%	1.79044		
NLO PDF						
k	Val	c'_n	Error(%)	Error	Shift	Match
0	6.20964	6.20964	99.7087%	6.19155	7.88946	✗
1	14.0991	12.4681	36.2912%	5.11673	5.01809	✓
2	19.1172	12.5326	15.119%	2.89033	3.16971	✗
3	22.2869	12.5106	7.69338%	1.71462		
NNLO PDF						
k	Val	c'_n	Error(%)	Error	Shift	Match
0	6.14041	6.14041	100.06%	6.14411	7.80439	✗
1	13.9448	12.2903	36.425%	5.07939	4.97416	✓
2	18.919	12.3358	15.1971%	2.87513	3.15341	✗
3	22.0724	12.3155	7.75452%	1.71161		

Fixed PDFs (NNLO) - Fitted λ - $l = 0$ Figure 4.5: Cross Section with NNLO PDF for $l = 0$, expansion parameter $\lambda\alpha_S$.

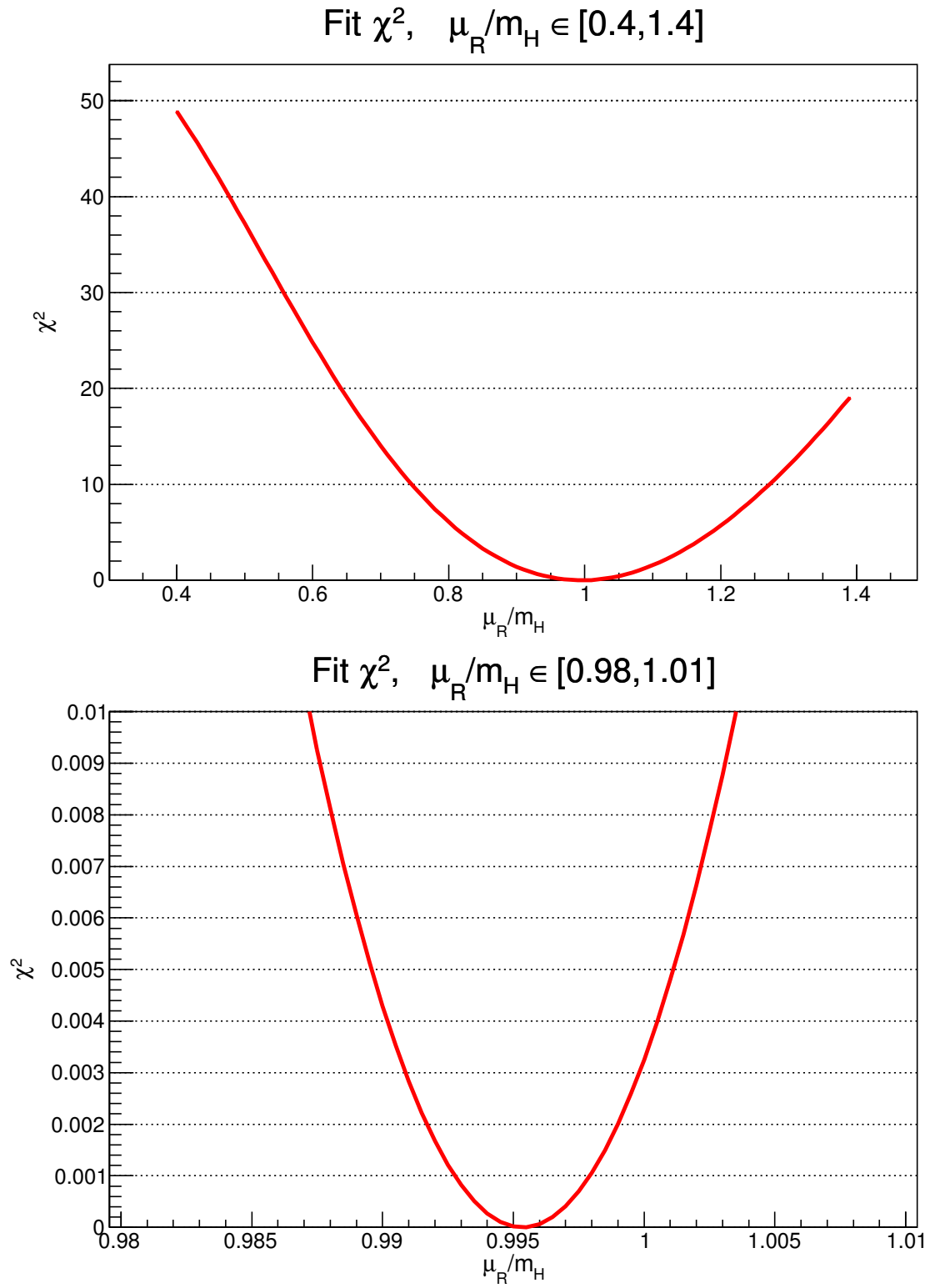
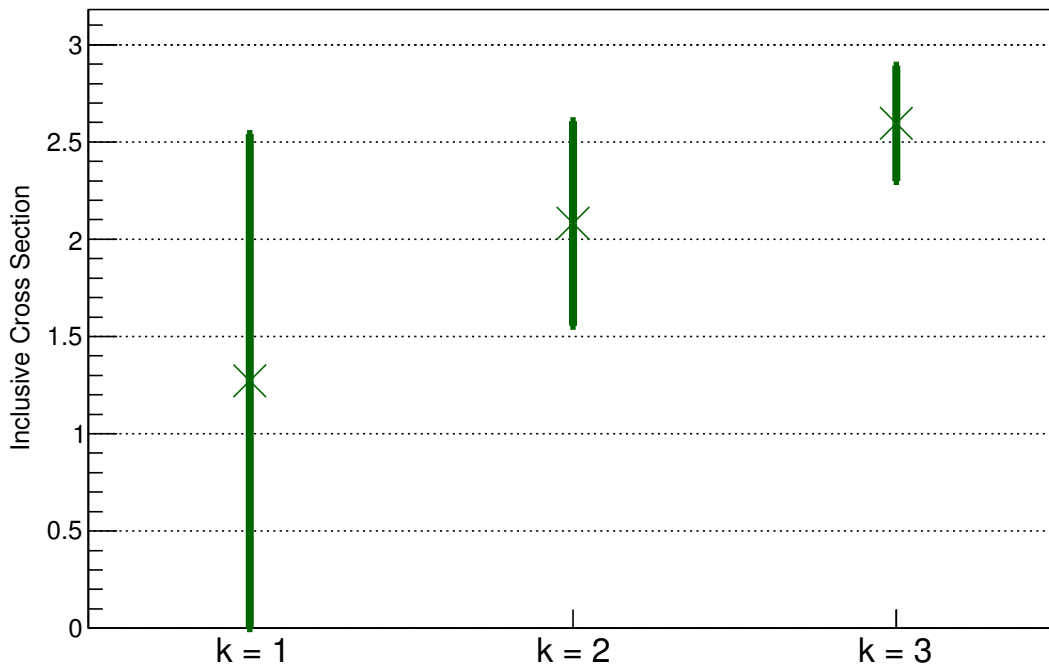
Figure 4.6: μ_R/m_H dependence of χ^2 .

Table 4.6: Fixed PDF results for $l = 1$, expansion parameter $\lambda\alpha_S$.

LO PDF						
k	Val	d'_n	Error(%)	Error	Shift	Match
1	1.28366	2.04218	99.0469%	1.27142	0.827458	✓
2	2.11112	2.09428	25.2514%	0.533087	0.519324	✓
3	2.63044	2.09109	11.3133%	0.29759		
NLO PDF						
k	Val	d'_n	Error(%)	Error	Shift	Match
1	1.27052	2.01061	99.5724%	1.26509	0.808113	✓
2	2.07863	2.02379	25.1794%	0.523386	0.510451	✓
3	2.58908	2.02299	11.3447%	0.293725		
NNLO PDF						
k	Val	d'_n	Error(%)	Error	Shift	Match
1	1.27099	2.00424	99.9257%	1.27004	0.810069	✓
2	2.08106	2.01437	25.3004%	0.526515	0.51355	✓
3	2.59461	2.01376	11.4287%	0.296529		

Fixed PDFs (NNLO) - Fitted $\lambda - l = 1$ Figure 4.7: Cross Section with NNLO PDF for $l = 1$, expansion parameter $\lambda\alpha_S$.

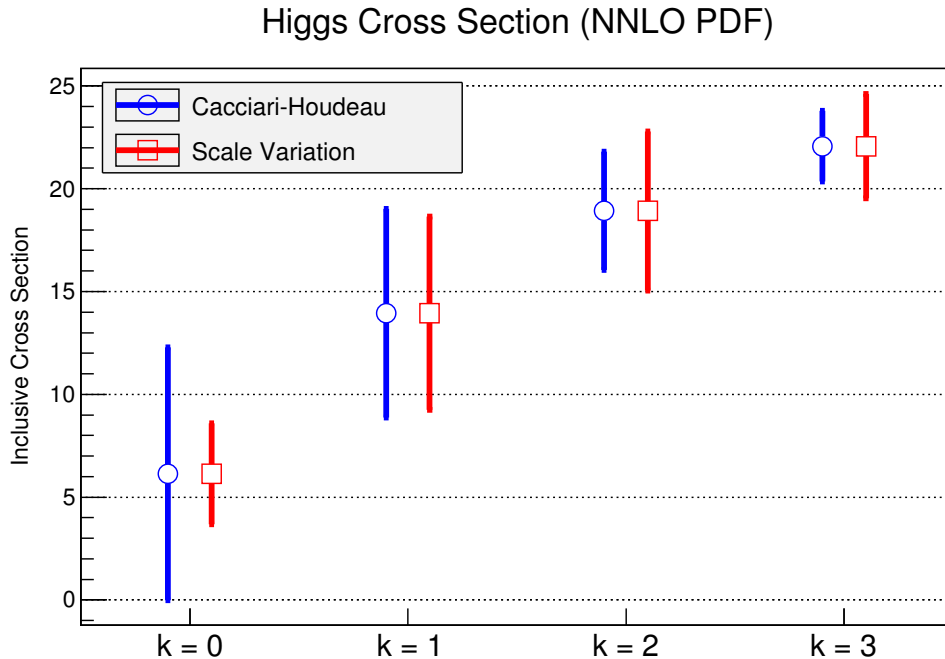


Figure 4.8: Comparison between the Cacciari-Houdeau and the scale variation method.

4.6 Comparison with scale variation

Among the advantages of the Cacciari-Houdeau model respect to the scale variation, besides the possibility of assigning a credibility interval to uncertainty estimates, there is its generality: the method can be applied to any kind of perturbative series. The application of the scale variation is instead limited to hard processes, where the cross section naturally depends on the renormalization scale. It would be harder to use it on the PDF or the luminosity series, which depend on the scale only indirectly.

However, a comparison between the two methods is still possible when the PDF set is kept fixed, say at NNLO, and uncertainty on σ_k are considered. In Figure 4.8, the scale variation and the Cacciari-Houdeau uncertainties are compared, showing good agreement from $k = 1$ onward. At $k = 0$, the Cacciari-Houdeau uncertainty is much larger, even though the next order is still outside the uncertainty band.

4.7 PDF impact

After having determined the PDF influence and the contribution coming exclusively from the Higgs production process, it is possible now to determine the impact of PDF theoretical uncertainties on the cross section, namely its ratio to the global uncertainty. Consider a perturbative series (“mixed”) in which the first term is σ_0 computed with LO PDF, then σ_1 with NLO PDF and σ_2, σ_3 with NNLO PDF. This is the series that is actually used for physical predictions. Figure 4.9 plots the Higgs cross section with the following uncertainty bands:

- **Fixed PDF:** $k = 0 \rightarrow$ Fixed PDF LO, $k = 1 \rightarrow$ Fixed PDF NLO, $k = 2, k = 3 \rightarrow$ Fixed PDF NNLO

Table 4.7: PDF uncertainty impact.

k	Fixed PDF	Fixed XS	Mixed	XS/PDF
0	99.1894%	17.735%	102.951%	0.178799
1	36.2912%	1.3457%	36.5713%	0.0370806
2	15.1971%	0.136564%	15.8141%	0.00898621
3	7.75452%	0.136593%	8.30255%	0.0176146

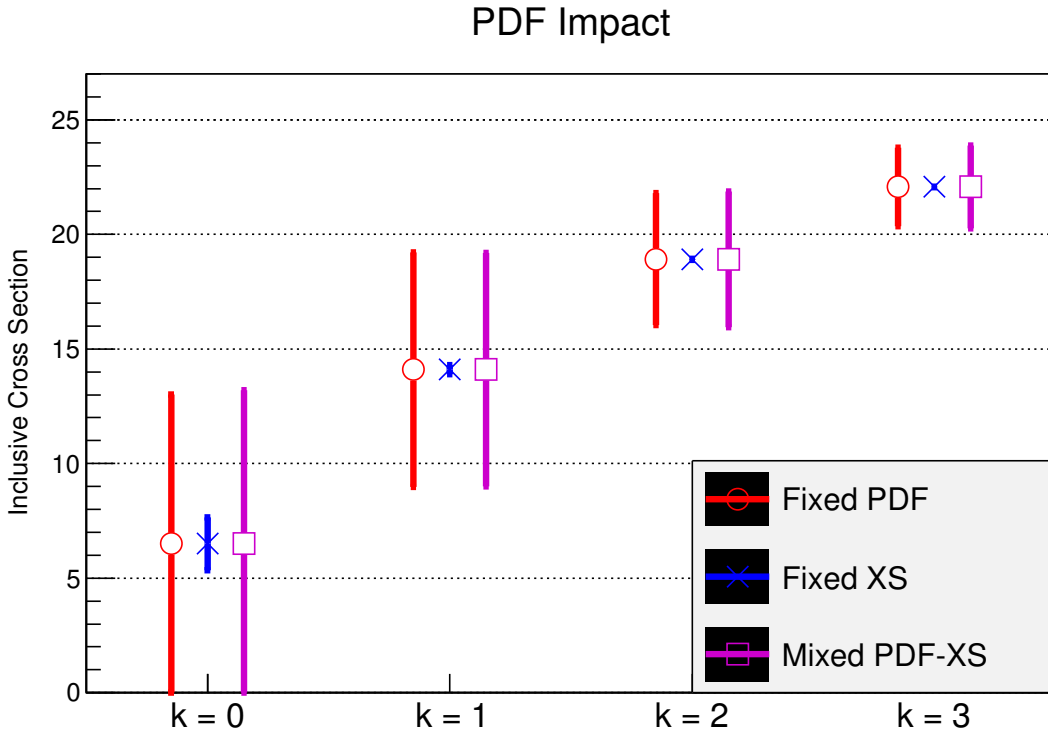


Figure 4.9: Impact of theoretical uncertainties on PDFs on Higgs cross section.

- **Fixed XS:** fixed cross section for each k
- **Mixed PDF-XS:** mixed series

where Fixed PDF contains the uncertainties coming from three different perturbative series, and is therefore substantially different from Mixed, which is treated as a single one. Table 4.7 collects numerical results and the ratio between Fixed XS and Fixed PDF uncertainty. This ratio represents therefore, for each k , the PDF contribution to the global uncertainty or, in other words, the effective *Impact of Theoretical Uncertainties of PDFs on the Higgs Cross Section*.

4.8 Concluding remarks

The main goal of this thesis was to analyse the impact of PDF uncertainties on the Higgs cross section. We have used the Cacciari-Houdeau method: a Bayesian approach which allows one to characterise the theoretical uncertainty of a perturbative calculation in terms of intervals of a given degree of belief.

First, we have considered the PDF and the gluon-gluon luminosity viewed as a perturbative series in α_S . The reliability of the method has been verified by studying theoretical uncertainty intervals on known terms, and comparing them to the subsequent orders. Then, we have computed theoretical uncertainties on the last known perturbative order, NNLO, which are smaller than 0.1%. Theoretical uncertainties on luminosity at $M_X = m_H$ have been found to be of a similar size.

After computing the cross section for Higgs production in gluon fusion, we have isolated the PDF dependence by fixing the matrix element and letting the PDF vary. We have found that relative theoretical uncertainties depend weakly on the order of the matrix element and, as one might have expected, they are very similar to those of the luminosity series: for the fixed N³LO cross section, they are 0.1%.

In order to determine the size of this correction in comparison to the uncertainty on the cross section itself, we have fixed the order of the PDF. In order to obtain perturbative coefficients roughly of the same size, we have rescaled the expansion parameter of this series from α_S to $\alpha_S \lambda$, with λ extracted from a fit. In good agreement with the scale variation method, theoretical uncertainties have been found to be 8%. Their ratio to the uncertainty arising from the PDF has been found to be, at N³LO, 0.02.

We conclude that the impact of theoretical uncertainties on PDFs on the Higgs cross section is negligible. Therefore a N³LO set of PDFs is not urgently required for this process, as the theoretical uncertainties of matrix element are by two order of magnitudes larger those on the PDFs.

Bibliography

- [1] R. K. Ellis, W. J. Stirling, and B. R. Webber, *QCD and collider physics*. Cambridge Univ. Press, Cambridge, UK, 1996.
- [2] <https://twiki.cern.ch/twiki/bin/view/LHCPhysics/CrossSections>
- [3] The **PDF4LHC** Working Group, *The PDF4LHC Working Group Interim Report*, [arXiv:1101.0536v1](https://arxiv.org/abs/1101.0536v1)
- [4] R. Plačakytė *Parton Distribution Functions* [arXiv:1111.5452v4](https://arxiv.org/abs/1111.5452v4)
- [5] A.D. Martin, W.J. Stirling, R.S. Thorne, G. Watt, Eur. Phys. J. C**63**, 189 (2009) [arXiv:0901.0002](https://arxiv.org/abs/0901.0002)
- [6] P. M. Nadolsky et al, Phys. Rev. D**78**, 013004 (2008) [arXiv:0802.0007](https://arxiv.org/abs/0802.0007)
- [7] R. D. Ball, L. Del Debbio, S. Forte, A. Guffanti, J. I. Latorre, J. Rojo and M. Ubiali, Nucl. Phys. B**838**, 136 (2010) [arXiv:1002.4407](https://arxiv.org/abs/1002.4407)
- [8] S. Forte and G. Watt, *Progress in the Determination of the Partonic Structure of the Proton*, [arXiv:1301.6754v1](https://arxiv.org/abs/1301.6754v1)
- [9] J. Collins, *Foundations of perturbative QCD*. Cambridge Univ. Press, Cambridge, UK, 2011.
- [10] J. C. Collins, D. E. Soper, G. Sterman, *Factorization of Hard Processes in QCD*, [hep-ph/0409313](https://arxiv.org/abs/hep-ph/0409313)
- [11] M. R. Whalley, D. Bourilkov, and R. C. Group, *The Les Houches accord PDFs (LHAPDF) and LHAGLUE*, [hep-ph/0508110](https://arxiv.org/abs/hep-ph/0508110)
- [12] J. Baglio and A. Djouadi *Predictions for Higgs production at the Tevatron and the associated uncertainties*, [arXiv:1003.4266v2](https://arxiv.org/abs/1003.4266v2)
- [13] Matteo Cacciari and Nicolas Houdeau, *Meaningful characterisation of perturbative theoretical uncertainties*, [arXiv:1105.5152v2](https://arxiv.org/abs/1105.5152v2)
- [14] O. Berger, *Statistical Decision Theory and Bayesian Analysis*, Springer-Verlag, 1985
- [15] <http://informafisica.it/c++/pdfset.tar.gz>
- [16] Richard D. Ball, Marco Bonvini, Stefano Forte, Simone Marzani, Giovanni Ridolfi, *Higgs production in gluon fusion beyond NNLO*, [arXiv:1303.3590](https://arxiv.org/abs/1303.3590)
- [17] <http://www.phys.ethz.ch/~pheno/ihixs/>